UNIVERSIDAD POLITÉCNICA DE MADRID
Escuela Técnica Superior de Ingenieros Industriales

High Power Bidirectional Wireless Electric Vehicle Chargers: Advanced Topology Solutions and Control Strategies

DOCTORAL THESIS

Submitted for the degree of Doctor by:

Nikola Mirković
Master's Degree in Electrical Engineering and Computer Science at Belgrade University

Madrid, 2024

UNIVERSIDAD POLITÉCNICA DE MADRID
Escuela Técnica Superior de Ingenieros
Industriales

Doctoral Degree in Electrical and Electronic Engineering

High Power Bidirectional Wireless Electric Vehicle Chargers: Advanced Topology Solutions and Control Strategies

DOCTORAL THESIS

Submitted for the degree of Doctor by:

Nikola Mirković
Master's Degree in Electrical Engineering and Computer Science at Belgrade University

Under the supervision of:
Prof. Dr. Pedro Alou Cervera
Prof. Dr. Miroslav Vasić Matić

Madrid, 2024

Title: High Power Bidirectional Wireless Electric Vehicle Chargers: Advanced Topology Solutions and Control Strategies
Author: Nikola Mirković
Doctoral Programme: Electrical and Electronic Engineering

Thesis Supervision:

Prof. Dr. Pedro Alou Cervera, Full professor, Universidad Politécnica de Madrid (Supervisor)

Prof. Dr. Miroslav Vasić Matić, Asociate professor, Universidad Politécnica de Madrid

External Reviewers:

Thesis Defense Committee:

Thesis Defense Date:

This thesis has been partially supported by the Spanish Ministry of Science and Innovation: Project PID2020-117582RB-I00 financed by MCIN/ AEI /10.13039/501100011033; and by the Spanish Ministry of Universities through the FPU grant intended for forming the future University Professors: Reference FPU21/05585

Acknowledgments

The last three years of doing the PhD thesis were very challenging for me, full of ups and downs, but certainly they will remain in a beautiful memory and become a story for the years to follow. Here I would like to show my appreciation to the people that have helped me on this journey.

First and foremost, I would like to thank my parents, Rajko and Rosanda, for raising me, and providing me with their guidance and undivided love and attention, shaping me into the man I am coming to be.

I would like to express my deepest gratitude to my tutors, prof. Pedro Alou and prof. Miroslav Vasić, who unselfishly shared their vast knowledge with me, guiding me through this three year research period, helping me nurture both knowledge and moral virtues.

This journey would have lasted longer if it was not for my friends and colleagues who supported me each day of this period. Among this group of people, special place belongs to Daniel Ríos Linares, my inseparable lab companion for all of this time. To my colleagues Dr. Đorđe Stojić, Luis Ruiz and prof. Alberto Delgado with whom I have performed my research together. To my colleagues from Centro de Electrónica Industrial: Carlos Jiménez, Miguel Astudillo, Gabriel Maldonado, Catalin Muntean, Xianghao Mo, Miguel Moya and Alejandro García. Special thanks I owe to our secretary Yolanda Rodrigo, who helped me combat the Spanish bureaucratic system.

Whenever I went home for vacations, I would receive support and encouragement from my friends to continue going down the path that I have chosen. Among many, I would like to mention: Nikola Stanić, Nemanja Pavlović, Aleksandar Savić, Natalija Milisavljević, Sonja Knežević and Filip Veljković.

I would also like to show my appreciation to prof. Dražen Dujić from EPFL who warmly welcomed me to his lab and showed me great hospitality for the duration of my three month research stay there.

My gratitude goes as well to the brotherhood of the Serbian medieval monastery of Studenica, for their immensive love, spiritual guidance and support over the last seven years.

Last on this list is the one that deserves to be mentioned first. To my soul-mate, to the queen of my heart, my beloved wife Anđelka, for all that we have endured together over the last three years - I love you.

Abstract

Wireless charging of the electric vehicles (EVs) is a contemporary topic that is becoming increasingly popular during the last decade, together with the growth of the EV share in the global market. Due to the lack of heavy-duty cables, contactless EV chargers, i.e., wireless chargers, offer seamless charging to the user. Based on the field that is used as the medium for power transfer, they can be divided into inductive and capacitive. This Thesis will focus only on the inductive ones.

One of the main advantages of the classical vehicles that rely on combustion engines over their electrical counterparts, is their charging time. Reducing the EV charging time would enhance their competitiveness on the market. For this reason, this Thesis mainly focuses on the high power solutions of the wireless EV chargers, being that the charging power is crucial for reducing the battery charging time.

Bidirectionality feature of the wireless EV charger is attractive when we consider the mentioned charger as the part of a local microgrid. If the charger is made bidirectional, than the EV is turned into an energy bank, capable of both receiving and providing energy if needed. Due to the low number of efficient bidirectional solutions in the state-of-the-art, two out of three charger topologies considered in this Thesis are bidirectional.

Wireless chargers based on the inductive power transfer (IPT) are known for their low efficiency levels as the consequence of the low coupling coefficient between the transmitter and receiver coils. With the ever-growing cost of energy, efficiency of power converters is one of the most important topics. With the increase in power rating of the charger, so does increase the need of its high efficiency. Being that the power ratings of the chargers presented in this work are ranging between several kilo-Watts up to several tens of kilo-Watts, one of the main goals of this Thesis is to present high efficiency solutions for their implementation.

With the previously said in mind, the main challenges related to IPT EV chargers that are addressed in this Thesis and the ideas that are outlined together with their accompanying scientific contributions are:

1. Efficiency of the IPT chargers and their compensation and functionality. A series (S-S-S) compensated three-coil bidirectional EV charger suitable for high power and high efficiency applications is proposed, allowing for high efficiency of the system and implementation of seamless control strategy. Contributions:
    1.1. A simple model of the three-coil IPT charger based on the T equivalent circuit, significantly facilitating the comprehension of the three-coil IPT systems.
    1.2. Tuning methodology for the used resonant capacitors, allowing for high efficiency and seamless control of the system.
    1.3. Design procedure of the proposed system.
2. AC/DC single-stage IPT chargers, allowing for integration of power conversion stages and higher power density of the system. A wireless charger based on the Three-Phase to Single-Phase Matrix Converter, suitable for compact medium power applications, is presented together with the accompanying modulation strategy. Contributions:
    2.1. A novel modulation strategy for the Three-Phase to Single-Phase Matrix Converter, that opens up space for seamless control of the considered system, while complying with grid standard in terms of high power factor and low distortion of the grid currents.
    2.2. The power flow control method between the primary and secondary sides that is free of any wireless communication between the microcontrollers that control the converters.
3. IPT chargers with compact poly-phase inductive link that allow for high power transferring capability and control of such systems. A single-stage, compact three-phase IPT system based on DD^{2}Q coil topology with the Reduced Three-Phase to Single-Phase Matrix Converter powering each phase, suitable for high power charging applications is proposed together with a method for its control. Contributions:
    3.1. A design procedure for an IPT system based on the DD^{2}Q coil topology
    3.2. Modulation of the Reduced Three-Phase to Single-Phase Matrix Converter allowing for grid compliance of the proposed system.
    3.3. A control strategy of the system that allows for equal power sharing between the phases both on primary and on the secondary side, under all possible alignment conditions.

Resumen

LA carga inalámbrica de vehículos eléctricos es un tema contemporáneo que se ha vuelto cada vez más popular en la última década, junto con el crecimiento de la cuota de los vehículos eléctricos en el mercado global. Debido a la falta de cables de gran potencia, los cargadores de vehículos eléctricos sin contacto, es decir, los cargadores inalámbricos, ofrecen una carga sencilla y comoda para el usuario. Según el elemento que se utiliza como medio de transferencia de energía, se pueden dividir en inductivos y capacitivos. Esta tesis se centrará únicamente en los inductivos.

Una de las principales ventajas de los vehículos convencionales de motores de combustión comparados con los vehículos eléctricos es su tiempo de carga. Reducir el tiempo de carga de los vehículos eléctricos mejoraría su competitividad en el mercado. Por esta razón, esta tesis se centra principalmente en soluciones de alta potencia para los cargadores inalámbricos de vehículos eléctricos, ya que la potencia de carga es crucial para reducir el tiempo de carga de la batería.

La característica de bidireccionalidad del cargador inalámbrico de vehículos eléctricos es atractiva cuando consideramos dicho cargador como parte de una microrred local. Si el cargador es bidireccional, el vehículo eléctrico se convierte en un banco de energía capaz de recibir y proporcionar energía según sea necesario. Debido al bajo número de soluciones bidireccionales eficientes en el estado actual de la tecnología, dos de las tres topologías de cargadores consideradas en esta tesis son bidireccionales.

Los cargadores inalámbricos basados en la transferencia de energía inductiva son conocidos por sus bajos niveles de eficiencia como consecuencia del bajo coeficiente de acoplamiento entre las bobinas transmisora y receptora. Con el creciente costo de la energía, la eficiencia de los convertidores de energía es un tema de gran importancia. Con el aumento de la potencia nominal del cargador, también aumenta la necesidad de que tenga alta eficiencia. Dado que las potencias nominales de los cargadores presentados en este trabajo oscilan entre varios kilovatios hasta varios decenas de kilovatios, uno de los principales objetivos de esta tesis es presentar soluciones de alta eficiencia para su implementación.

A partir de lo anteriormente expuesto, las principales ideas presentadas en esta tesis, junto con sus contribuciones científicas correspondientes, son las siguientes:

1. Eficiencia de los cargadores IPT y su compensación y funcionalidad. Se propone un cargador bidireccional de EV con compensación en serie (S-S-S) de tres bobinas, adecuado para aplicaciones de alta potencia y alta eficiencia, lo que permite una alta eficiencia del sistema y la implementación de una estrategia de control sencilla. Contribuciones:
    1.1. Un modelo simple del cargador de IPT de tres bobinas basado en el circuito equivalente T, facilitando significativamente la comprensión de los sistemas de IPT de tres bobinas.
    1.2. Metodología de ajuste para los condensadores resonantes utilizados, permitiendo una alta eficiencia y un control sin problemas del sistema.
    1.3. Procedimiento de diseño del sistema propuesto.
2. Cargadores IPT de una sola etapa AC/DC, que permiten la integración de etapas de conversión de potencia y una mayor densidad de potencia del sistema. Se presenta un cargador inalámbrico basado en un Convertidor Matricial de Tres Fases a Una Fase, adecuado para aplicaciones compactas de potencia media, junto con la estrategia de modulación correspondiente. Contribuciones:
    2.1. Una estrategia novedosa de modulación para el convertidor de matriz trifásica a monofásica, que abre espacio para un control sin problemas del sistema considerado, al tiempo que cumple con las normas de la red en términos de alto factor de potencia y baja distorsión de las corrientes de la red.
    2.2. Método de control del flujo de energía entre los lados primario y secundario que prescinde de cualquier comunicación inalámbrica entre los microcontroladores que controlan los convertidores.
3. Cargadores IPT con un enlace inductivo polifásico compacto que permiten una alta capacidad de transferencia de potencia y el control de dichos sistemas. Se propone un sistema IPT compacto de tres fases y una sola etapa, basado en una topología de bobina DD^2Q con el Convertidor Matricial Reducido de Tres Fases a Una Fase alimentando cada fase, adecuado para aplicaciones de carga de alta potencia, junto con un método para su control. Contribuciones:
    3.1. Modulación del Convertidor de Matriz Trifásica a Monofásica Reducido que permite la conformidad con la red del sistema propuesto.

3.2. Una metodología híbrida para la técnica de estimación de la matriz de impedancia, basada en simulaciones para una estimación aproximada y perturbación y observación para ajustar finamente la estimación aproximada.

3.3. Una estrategia de control del sistema que permite un reparto equitativo de potencia entre las fases tanto en el lado primario como en el secundario, bajo todas las condiciones posibles.

Contents

List of Tables

List of Figures

Acronyms

3-D 3-Dimension.

AC Alternating Current.

AC/AC Alternating Current to Alternating Current.

BMS Battery Management System.

CC Constant-Current.

CPT Capacitive Power Transfer.

CV Constant-Voltage.

DAB Dual Active Bridge.

DC/DC Direct Current to Direct Current.

DC Direct Current.

EMF ElectroMagnetic Field.

EMI Electromagnetic Interference.

EU European Union.

EV Electric Vehicles.

FEA Finite Element Analysis.

GA Ground Assembly.

G2V Grid to Vehicle.

IPT Inductive Power Transfer.

LFM Linear Feet per Minute.

MCU MicroController Unit.

PF Power Factor.

PFC Power Factor Correction.

PI Proportional-Integral.

P-P Parallel-Parallel Resonant Topologies.

P-S Parallel-Series Resonant Topologies.

PWM Pulse Width Modulation.

RMS Root Mean Square.

RTSMC Reduced Three-phase to Single-phase Matrix Converter.

SAE Society of Automotive Engineers.

SiC Silicon Carbide.

S-P Series-Parallel resonant topology.

S-S Series-Series resonant topology.

SSMC Single-phase to Single-phase Matrix Converter.

SVM Space Vector Modulation.

THD Total Harmonic Distortion.

TSMC Three-phase to Single-phase Matrix Converter.

VA Vehicle Assembly.

V2G Vehicle to Grid.

UAV Underwater Autonomous Vehicles.

WPT Wireless Power Transfer.

ZVS Zero Voltage Switching.

CHAPTER 1

Introduction

> The discovery of an important need is almost as important as the invention which satisfies this need.
>
> Mihajlo Idvorski Pupin

1.1 Motivation

In the last couple of decades, there has been a sharp increase in human awareness of the ongoing climate change. The average yearly global temperature throughout the 20^{th} and the beggining of the 21^{st} century, is shown in Fig. 1.1a, portraying for the acute problem of global warming [1], [2]. It is well known that one of the main pollutants contributing to the greenhouse effect and consequentally leading to the temperature increase is carbon-dioxide CO_2 [3]. Fig. 1.1b depicts the amount of carbon emitted into the atmosphere over the last century. One of the first and most significant events related to combating the climate change was the Kyoto Summit in 1997, where representatives of more than 160 countries agreed to start reducing the greenhouse gases, making this one of the main goals of humanity for the following century [4].

Burning fossil fuels substantially contributes to the climate crisis. With the worldwide increase of life standard, during the last 50 years, number of vehicles is constantly on the rise. For this reason, there has been a significant effort on the global scale towards replacing the classical vehicles relying on the internal combustion engine, with vehicles that would not rely on fossil fuels, such as hydrogen or electrical vehicles (EVs) [5]. The current price of technology of the first ones, makes them unavailable for mass-use, although constant efforts are being made in this area towards reducing the price of

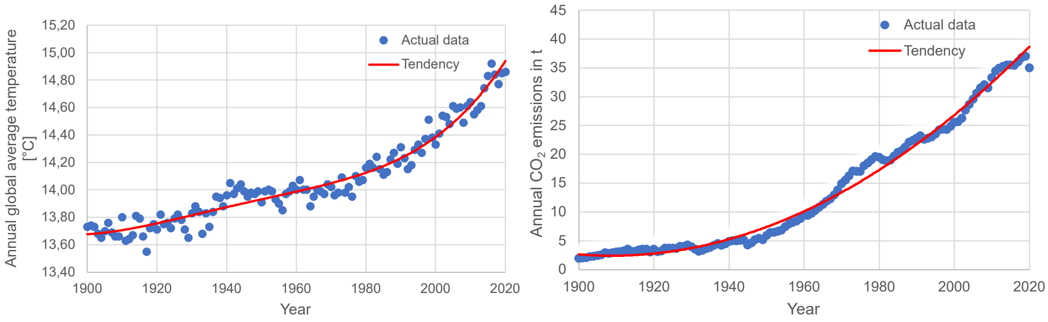

(a) (b)

Figure 1.1: a) Annual global average temperature over the years b) Annual CO_2 emissions over the years

hydrogen powered vehicles [6]. With a substantially lower price comparing to hydrogen vehicles, the EVs are more present in the market. Fig. 2 gives the share of electrical vehicles among the registered cars in the European Union (EU) in 2014 and 2022 [7].

One of the main advantages of vehicles relying on internal combustion engine over EVs is their low charging time. Companies and researchers are making continuous efforts on decreasing the charging of EVs by increasing the charging power [7]. Table 1.1 shows the list of companies and the power of their ultra-fast chargers that they offer. All of the mentioned chargers, as well as the vast majority of those in current use, are classical plug-based chargers, where it is necessary to manipulate heavy-duty cables in order to connect or disconnect the vehicle from the charger.

Contactless chargers for EVs, also referred to as wireless chargers, present a potential solution for seamless charging of EVs, as they do not require of the user to handle any cables during the charging process. It is possible to categorize all of the wireless EV chargers in three ways. Regarding the coupling field used for transferring power they can be divided in:

1. Inductive chargers, relying on the inductive coupling between the coil assemblies on the ground and on-board the vehicle - Inductive Power

Company	Name	Rated power of the ultra-fast charger	Battery voltages
Siemens	SICHARGE-D	400 kW	150 V - 1 kV
Delta	UFC500	500 kW	200 V - 920 V
Blink Charging	HYC 400	400 kW	150 V - 1 kV
EVBox	Troniq High Power	400 kW	150 V - 980 V
ABB	Terra 360	360 kW	150 V - 920 V
Tritium	PK350	350 kW	up to 920 V

Table 1.1: List of companies and the rated power of their ultra-fast chargers

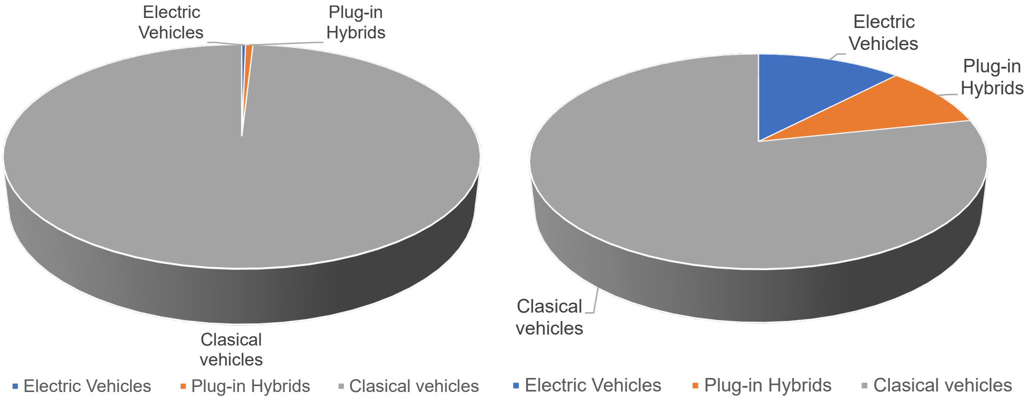

(a) (b)

Figure 1.2: Share of Electric Vehicles and Plug-in Hybrid Vehicles in the EU market a) 2014, less than 1% b) 2022, 21.6%

Transfer (IPT) [8], [9].

2. Capacitive chargers, relying on the capacitive coupling between the large metal plates on the ground and on-board the vehicle - Capacitive Power Transfer (CPT) [10]–[13].

Inductive chargers are more common to be encountered as capacitive coupling structures are rather big in size, usually employed in small air-gap applications, have higher voltages and operating frequencies, offer lower efficiency and lower power transferring capability when compared to their inductive counterparts that have same dimensions [14]–[17]. From the point of view of mobility, wireless EV chargers can be sorted out in:

1. Dynamic chargers, intended for charging the vehicle while it is on the move [18], [19].
2. Static charger, intended for charging the vehicle while it is parked [20], [21].

Dynamic charging utilizes the contactless nature of the energy transfer to its full extents, as it enables not only seamless handling, but rather it allows for reduction in battery size and consequently reduction in vehicle cost [22], [23]. On the other hand, dynamic charging requires development of highly expensive road infrastructure, which negates the benefit of reduced vehicle cost.

The last classification of wireless chargers is related to the power flow direction and, in that sense, it is possible to differentiate between:

1. Unidirectional chargers, offering only the possibility to transfer power from the electrical grid to vehicle (G2V mode of operation).

2. Bidirectional chargers, offering possibility of transferring power both from grid to vehicle, as well as from vehicle back to the grid (V2G mode of operation).

With the ongoing development of DC microgrids and distributed power generation, enhancing the EV charger with the bidirectionality feature turns every EV into an energy bank, capable of both receiving and providing power when necessary.

1.2 Objectives

This Thesis focuses on static EV chargers that utilize IPT principles for bridging the air gap between the ground and EV. Challenges of the IPT technology that are addressed in this work are:

1. Efficiency of the IPT systems and compensation of the inductive link.
2. Power flow control of IPT chargers.
3. Integration of power conversion stages through utilization of advanced converter topologies.
4. Control of compact poly-phase IPT chargers.

Four topics related to previously stated challenges tied to IPT chargers will be covered in this Thesis:

1. Compensation of the inductive link based on an auxiliary coil and resonant circuit.
2. Seamless method for achieving synchronous operation between converters energizing the system.
3. Single-stage AC/DC IPT charging solutions based on different matrix converter topologies.
4. IPT charger with a three-phase DD^{2}Q inductive link.

When compared to the classical plug-based chargers, IPT chargers have lower system efficiency due to the weakly coupled coils of the ground and vehicle assemblies. In this Thesis, a compensation strategy using an intermediate coil is proposed, suitable for high-power, bidirectional chargers, offering high system efficiency in the entire alignment tolerance area.

Wireless IPT chargers that can be encountered in the current state-of-the-art, usually comprise several power conversion stages, resulting in bulky solutions with low system efficiency. In order to overcome this issue, a bidirectional, single-stage solution is proposed, utilizing a Three-phase to Single-phase Matrix Converter (TSMC), with a novel modulation strategy that was devised for this purpose.

When high power delivery is required a poly-phase system comes as a natural solution. An IPT system comprising a three-phase inductive link is presented, having a single energy conversion stage between the electrical grid and the EV battery. Design methodology for the inductive link is presented, as well as the modulation strategy for the employed grid-interfacing converter. Control methodology for balancing the power distribution across the phases in the case of misalignment between the transmitter and receiver structures is proposed, thus overcoming one of the biggest obstacles when it comes to implementation of poly-phase IPT system in EV applications.

1.3 Outline of the Thesis

This Thesis has six chapters in total. Besides the Introduction chapter, where the motivation for this work is stated together with the objectives, there are five more chapters, each describing a certain topic related to IPT chargers, as it was stated above:

Chapter 2 gives the overview of the current state-of-the-art, pointing out to the existing solutions in the domain IPT chargers, that can be encountered in the literature, and that are related to the compensation strategies of the inductive link, single-stage charger solutions and IPT systems with three-phase inductive link.

Chapter 3 describes an IPT system compensated using an intermediate coil and resonant capacitors. A simple electrical model for the considered system is proposed and derived, based on a three-winding transformer, significantly facilitating the understanding and analysis of such system. Furthermore, design methodology of such a system, together with the tuning strategy for the resonant capacitors, are proposed, suitable for high-power charging, and allowing for high efficiency of the system even in the case of misalignment. Experimental prototype is realized and results of the proposed ideas are presented for power levels of up to 37 kW, and efficiencies ranging between 91.7% to 96.4%, for a 800 V EV battery.

Chapter 4 deals with a bidirectional single-stage IPT charger employing a TSMC for interfacing the grid. A novel modulation strategy for the given converter is presented, allowing for low total harmonic distortion (THD) of the grid currents and high power factor (PF). Experimental validation is given on a 3.6 kW prototype, achieving 0.975 PF and 3.2% THD of the grid currents, with more than 94.5% efficiency for a 400 V EV battery.

Chapter 5 presents a solution for high-power, single-stage IPT charger, with a three-phase inductive link based on DD^{2}Q coil topology. Reduced TSMC topology is used for interfacing each of the phases of the inductive link with the grid. Modulation strategy for the given converter is proposed, allowing for compliance of the given system with the grid code. Design procedure of the inductive link of a three-phase IPT with DD^{2}Q coil topology is presented. Problem of power balancing between the phases of the IPT link is discussed and control strategy is proposed to deal with this issue. A 24 kW prototype has been developed in order to validate the proposed solutions, showing system compliance with the grid code and achieving efficiency of 86.42% for charging a 400 V EV battery.

In **Chapter 6**, a summary of the work presented in this Thesis is given highlighting the contributions. Also, proposal is made for the future work, intended to give guidance for the enhancement of the concepts presented in this Thesis.

CHAPTER 2

State-of-the-Art

> Nothing is too wonderful to be true, if it be consistent with the laws of nature.
>
> Michael Faraday

One of the biggest challenges that the contemporary IPT systems are facing is the compensation of the inductive link. Namely, one can contemplate the coupled coils of the IPT system as a core-less transformer, where the coupling coefficient for the EV charging applications, according to the current SAE standard proposal [24], is predicted to be between 0.08 and 0.25. Due to this low values of the coupling factor, this system cannot be utilized unless it is compensated. Fig. 2.1a shows the typical depiction of wireless EV charging inductive link with two coupled coils, while the electrical schematic and the T-transformer model of these coils is given in Fig. 2.1b and Fig. 2.1c, respectively. If we assume that the self-inductances of the primary and of the secondary coil are L_p and L_s, and that the coupling coefficient between the two is k, than, the parameters of the T model can be expressed as:

$$L_\mu = kL_p \tag{2.1}$$

$$L_{\gamma p} = (1-k)L_p \tag{2.2}$$

$$\frac{n_p}{n_s} = \sqrt{\frac{L_p}{L_s}} \tag{2.3}$$

$$L_{\gamma s} = (1-k)L_s \tag{2.4}$$

Having in mind the previously mentioned range of coupling coefficient values, it is obvious that it is necessary to compensate the inductive link in order to obtain a useful system with a certain desired functionality.

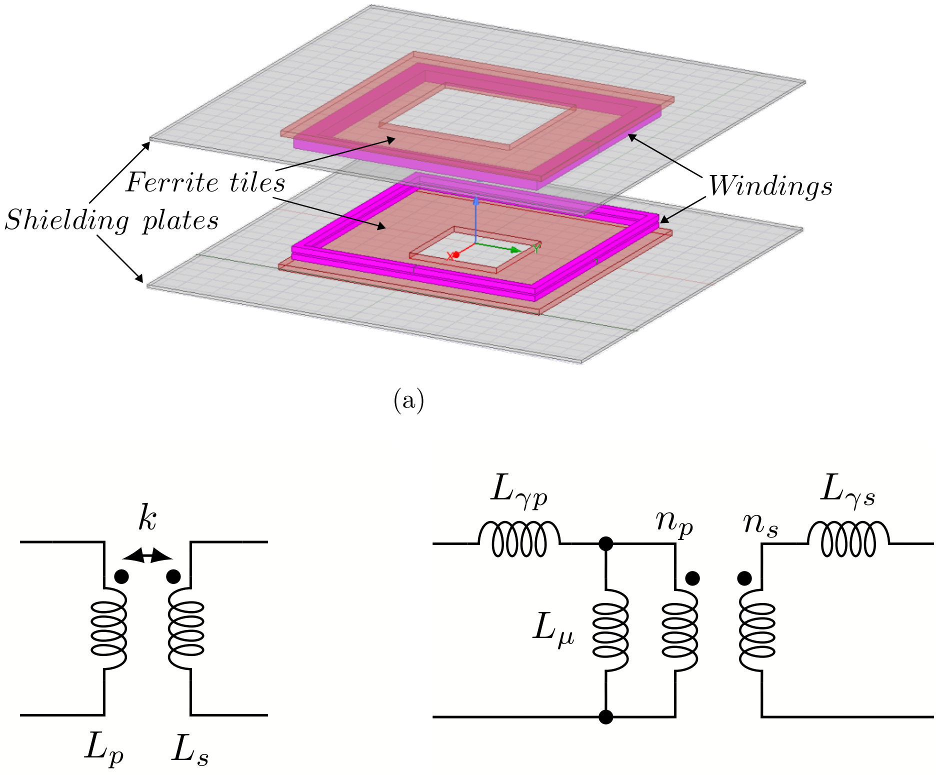

(a)

(b)

(c)

Figure 2.1: a) Typical depiction of the inductive link, b) Coupled inductors, c) T-transformer model of the coupled inductors

2.1 Compensation strategies of the inductive link

A lot of different compensation strategies have been devised and can be encountered in the literature. The most common one,being also the simplest one, is the series-series (S-S) compensation strategy [25]–[30], comprising two additional capacitors added in series with the primary and secondary coils as it is given in the Fig. 2.2a. Two different tuning methods for the added capacitors can be encountered in the literature. In the less-common one that can be seen in [26], serial capacitors are tuned to resonate with the leakage inductances at the inverter operating frequency:

$$C_p = \frac{1}{\omega^2 L_{\gamma p}} \tag{2.5}$$

$$C_s = \frac{1}{\omega^2 L_{\gamma s}} \tag{2.6}$$

where ω is the fundamental angular frequency. Compensating the system in this way, output voltage is independent on the load, achieving the so-called constant-voltage (CV) output characteristic. In EV charging applications it is impossible to precisely predict the value of the coupling coefficient due to the existence of misalignment between the coils of ground assembly (GA) and vehicle assembly (VA). Having this in mind, and a very narrow range of operating frequencies predicted by the current SAE standard proposal that is between 80 kHz and 90 kHz, this type of compensation is more suitable for applications where it is possible to foresee the exact value of the coupling coefficient between the two coils.

The other, more common way of tuning serial capacitors, when it comes to the S-S compensation strategy, is tuning them to resonate with the self-inductances of the coils at the inverter operating frequency:

$$C_p = \frac{1}{\omega^2 L_p} \tag{2.7}$$

$$C_s = \frac{1}{\omega^2 L_s} \tag{2.8}$$

By tuning the serial capacitors this way, a structure known as *gyrator* is obtained, that is shown in Fig. 2.3. It is possible to mathematically show that, in such system, placing a voltage excitation on one side, a current response will be produced on the other one and vice-versa. Relation between the input voltage and output current, or the input current and output voltage, is given by the following equations:

$$U_p = j\omega k\sqrt{L_p L_s} I_s \tag{2.9}$$

$$U_s = j\omega k\sqrt{L_p L_s} I_p \tag{2.10}$$

Normally, excitations that we have at our disposal are voltage in nature, so, it is clear that applying this compensation method, a constant-current (CC) output characteristic is obtained, i.e., constant current is seen at the output of the vehicle-side resonant circuit. This is very beneficial in all battery charging applications including EV charging as well. Also, the system always stays at resonance, independently on the alignment of the coils.

Besides the S-S compensation strategy, three more compensation strategies can be singled out from the group of fundamental ones. Those are: Series-Parallel (SP), Parallel-Series (PS) and Parallel-Parallel (P-P) and they are shown in Figures 2.2b - 2.2d, respectively [31]. The first two of these topologies tend to have CV output characteristic, while the last one has CC output characteristic. Detailed analysis of the functionality of the IPT systems compensated with these compensation strategies can be found in [32]. Despite their simplicity, these compensation strategies are not commonly encountered, as they are sensitive to the existence of the DC component in the excitation voltage, and to high dV/dt during switching transitions, due to parallel capacitors.

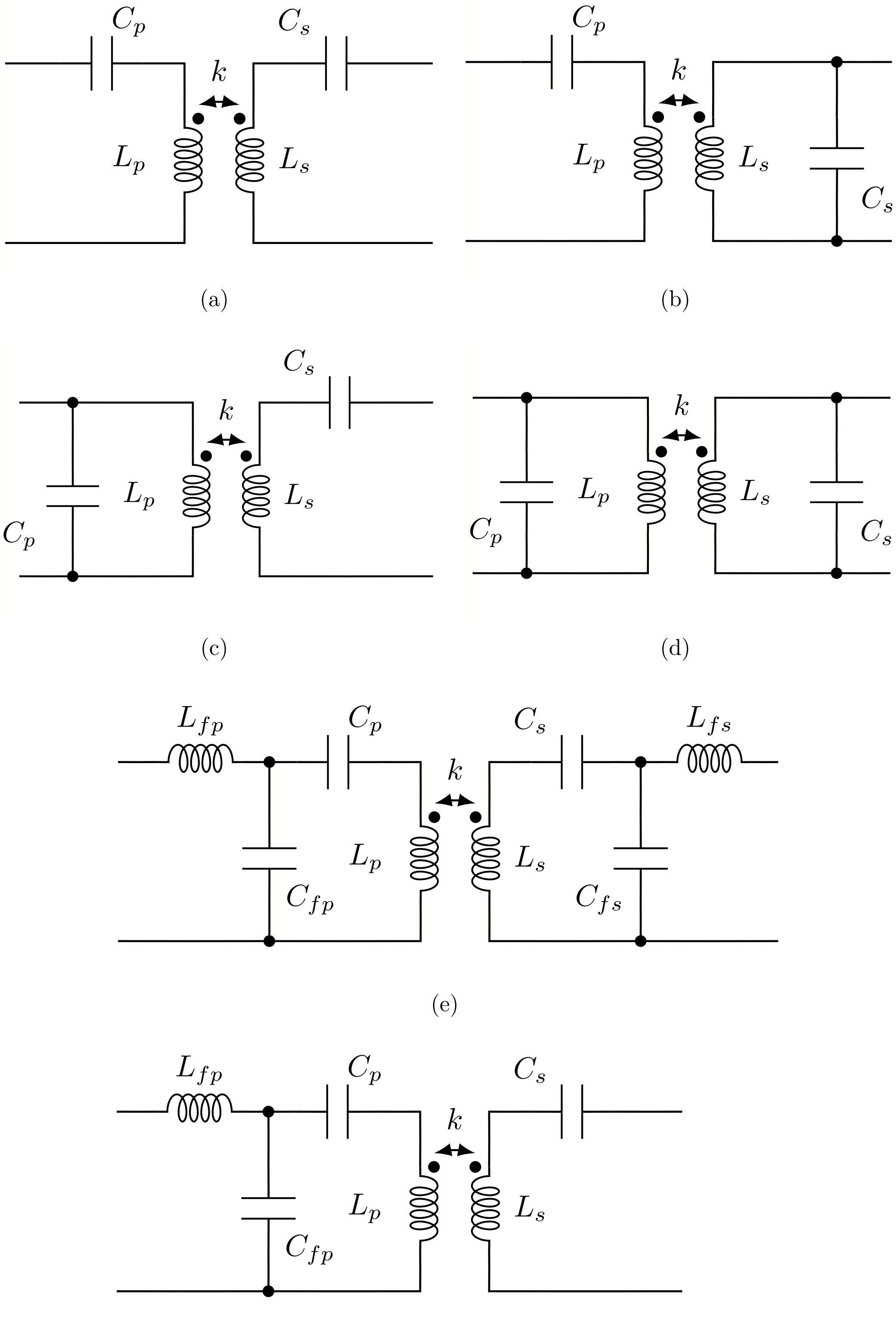

(a) (b) (c) (d) (e) (f)

Figure 2.2: Common compensation topologies a) Series-Series (S-S), b) Series-Parallel (S-P), c) Parallel-Series (P-S) d) Parallel-Parallel (P-P) e) Double-sided LCC f) LCC-S

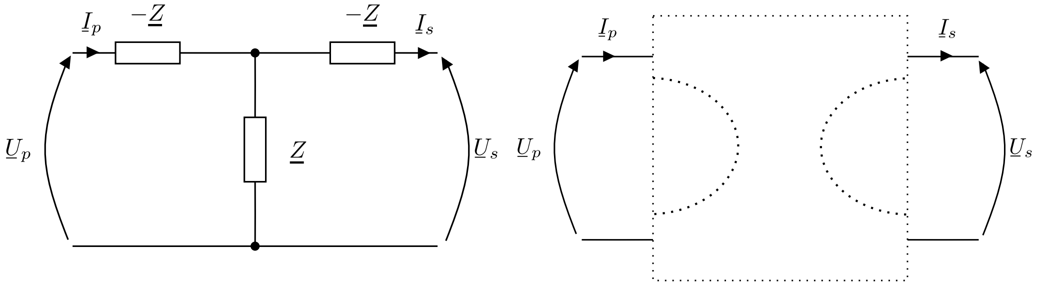

(a) (b)

Figure 2.3: Gyrator a) Structure and b) Symbol

From the group of more complex compensation strategies, the application of double-sided LCC compensation strategy [33] is present throughout the literature [34]–[37]. Depiction of IPT link compensated in this manner is given in Fig. 2.2e. By introducing more reactive elements to the system, higher efficiency of the system is achieved, even in the conditions of misalignment [33], all at the cost of reduced simplicity of the system. System parameters are tuned according to the following equations:

$$1 = \frac{1}{\omega^2 L_{fp} C_{fp}} \tag{2.11}$$

$$1 = \frac{1}{\omega^2 (L_p - L_{fp}) C_p} \tag{2.12}$$

$$1 = \frac{1}{\omega^2 L_{fs} C_{fs}} \tag{2.13}$$

$$1 = \frac{1}{\omega^2 (L_s - L_{fs}) C_s} \tag{2.14}$$

Such system will exhibit a CC output characteristic, as it can be regarded as a cascade connection of three gyrators, as depicted in Fig. 2.4. For the reason of its high efficiency, this compensation method is often used in high-power IPT charging applications.

Also, it is possible to find compensation strategies that are a combination of some of the basic ones such as series, on one side of the system, and a complex LCC on the other side, i.e., the LCC-S compensation strategy [38]–[40], that is given in Fig. 2.2f. Parameters of the system are tuned according to the following equations:

$$1 = \frac{1}{\omega^2 L_{fp} C_{fp}} \tag{2.15}$$

$$1 = \frac{1}{\omega^2 (L_p - L_{fp}) C_p} \tag{2.16}$$

$$1 = \frac{1}{\omega^2 L_s C_s} \tag{2.17}$$

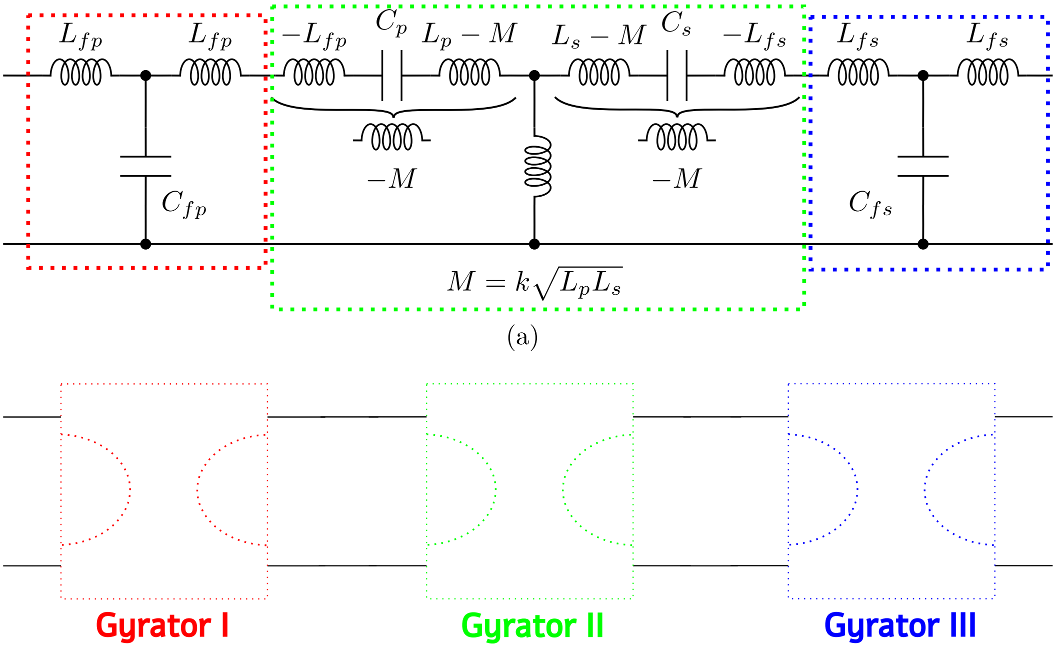

(a)

(b)

Figure 2.4: Functional diagram of the double-sided LCC compensation strategy

System compensated using this compensation strategy has a CV output characteristic as it can be looked upon as serial connection of two gyrators as it is shown in Fig. 2.5. Both double-sided LCC, and LCC-S compensation methods are alignment invariant as the elements of the system are tuned to resonate independently on the coupling between the transmitter and receiver coils.

Alongside with the research tied to the previously mentioned compensation strategies that are intended for two-coil systems, IPT systems with three [41]–[52] and four [53]–[58] coils were analyzed. According to [59], four-coil systems are more suitable for high efficiency, low power applications, as they offer higher power transfer efficiency but lower power delivered to the load comparing to the three-coil systems. While offering slightly reduced efficiency comparing to the four-coil systems, three-coil systems prove themselves more suitable for applications requiring high power transfer capability, i.e. they present a potential candidate for EV charging applications. Furthermore, work [60] compares efficiencies of the SS compensated system, LCC-S compensated system and the three-coil system, showing that the last two have similar efficiencies, both significantly larger than the efficiency of the first one. Also, works [61], [62] show the possibility of increased power transfer capability of the three-coil system under misalignment conditions. All of the previously stated articles provide a reasonable argument for continuing research of the three-coil systems in EV charging applications.

In the current state-of-the-art there is a significant number of works investigating the three-coil IPT systems. Authors in [41], [47], [51] analyze

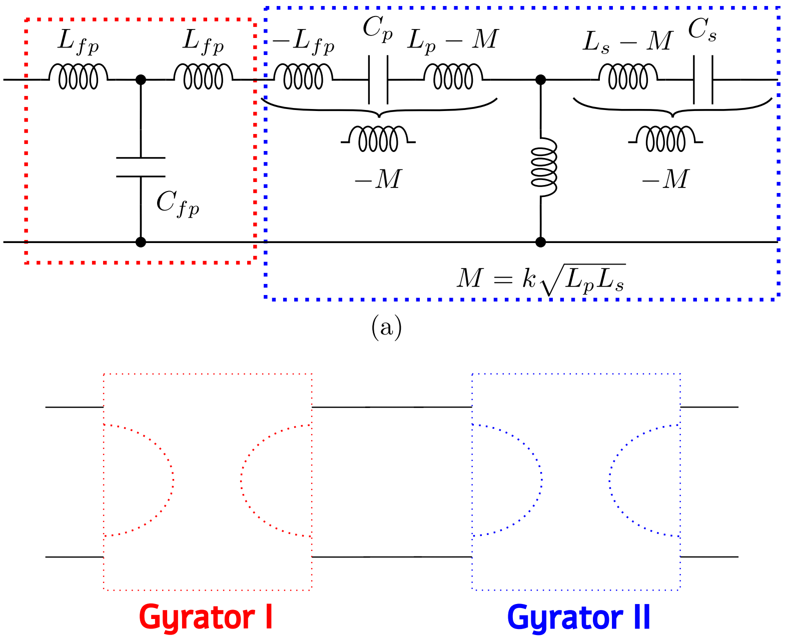

(a)

(b)

Figure 2.5: Functional diagram of the LCC-S compensation strategy

and compare two-coil and three-coil systems, proving that it is possible to make a three-coil IPT system more efficient than a two-coil one, as well as that the three-coil IPT system exibits higher efficiency stiffness against load variations and reduced EMF emissions. Being that the most common way of charging the contemporary Li-ion batteries is the constant-current/constant-voltage (CC/CV) charging profile, that is shown in Fig 2.6a, a lot of the works related with the three-coil IPT systems [44], [46], [48]–[50] propose a certain hybrid topology or control technique that would allow the CC/CV charging of the EV battery. The IPT system with an additional diode rectifier added to the assistive coil circuit is given in [44], allowing for the seamless change between CC and CV modes of operation. In [46] authors propose a hybrid topology, adding 2 four-quadrant switches and several passive elements in order to achieve different resonance behaviors of the system in dependence

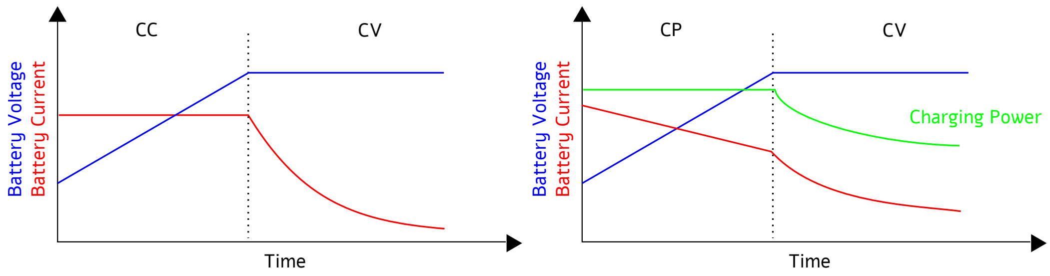

(a) (b)

Figure 2.6: Charging profiles of the Li-ion battery a) CC/CV b) CP/CV

on the CC or CV charging mode of operation. Similar approach to this one is seen in [49]. Somewhat simpler solution is present in [48], comprising a reconfigurable topology that can change between the two-coil and three-coil topologies, depending whether CC or CV mode of operation is required. Another example of a reconfigurable topology is present in [63], where authors propose a system that can change between two-coil, three-coil and four-coil topology, and in that way preserve the system efficiency at high level over a large span of varying distances between transmitter and receiver. On the other side, in [50] authors have applied a frequency control to the three-coil S-S-P compensated system in order to change between different charging modes. Frequency control of a three-coil IPT is as well present in [45], where authors propose an optimal design method of the three-coil IPT system using the second resonance frequency with the bifurcation phenomenon. A novel S-S-LCLCC compensation method for three-coil IPT is proposed in [42], showing improved misalignment and efficiency stiffness of the IPT system. A very interesting approach when it comes to the three-coil IPT systems can be seen in [43] where authors propose a special design of the magnetic coupler to avoid unwanted coupling between certain windings, and using the S-S-S compensation strategy achieve load-independent CV charging characteristics. When it comes to the matter of bidirectionality, all of the previously mentioned works are unidirectional. Complexity of some of them is relatively high as they incorporate additional four-quadrant switches and several passives in order to achieve CC/CV charging operation. On the other hand, others rely on varying the operating frequency, making those solutions challenging for implementation in the EV charging applications as the current standard proposal predicts very narrow window of operable frequencies of the system. From the point of view of the charging method, there are other charging methods mentioned in the literature, such as constant-power/constant-voltage (CP/CV) that is shown in Fig 2.6b [64]–[66], or pulsed-current charging methods [67], [68]. While the latter one is still being investigated the first one has known advantages over the CC/CV charging method such as longer battery lifecycle and utilizing maximum power transfer capacity of the charger.

2.2 Single-stage AC/DC IPT chargers

In the previous section, a necessity for the compensation of the inductive link was explained, and the most common approaches for overcoming this challenge, that can be encountered in the literature, have been outlined. When it comes to converter topology used for energizing the inductive link and powering the entire IPT system, typical schematic of a grid-connected solution, can be represented as shown in Fig. 2.7. It consists of two [69]–[71] or three stages [72], [73]:

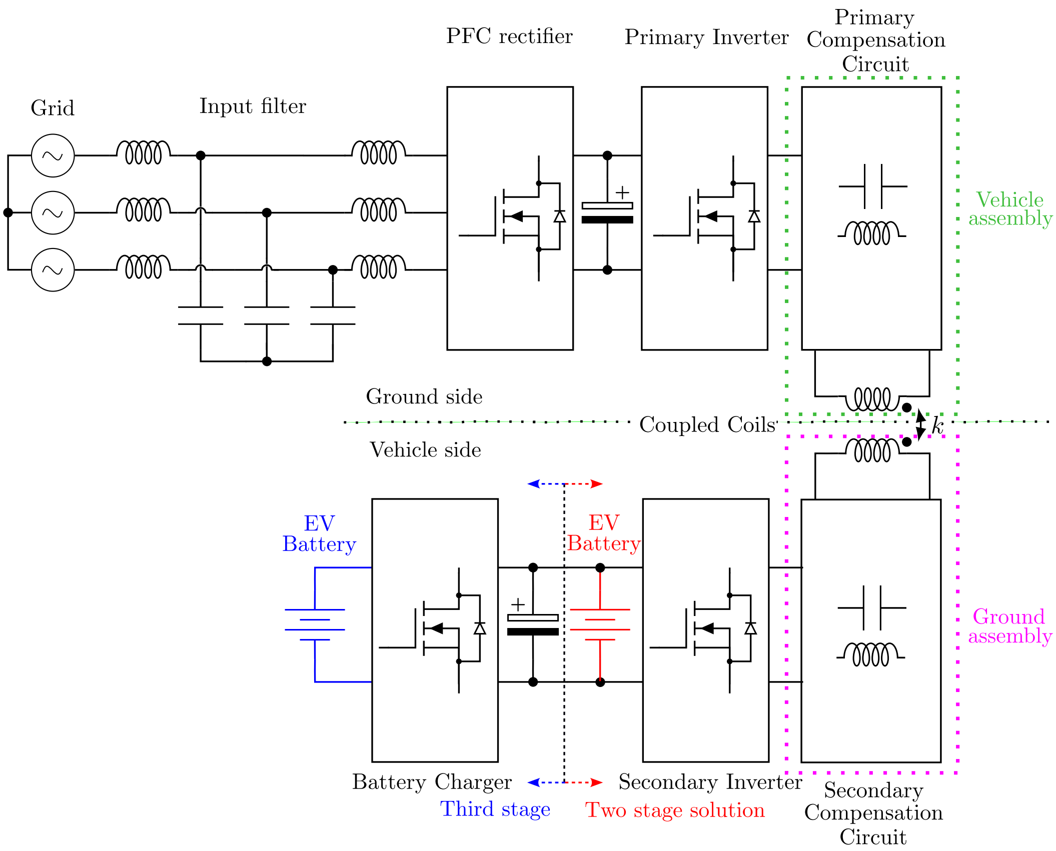

Figure 2.7: Simplified schematic of a typical bidirectional IPT system

- Interfacing the grid there are the PFC rectifier and input filter.
- Following comes the resonant DC/DC stage, comprising the coils of the inductive link. Primary inverter is connected to the primary coil and its corresponding compensation circuit, i.e., the GA.
- On the side of the vehicle, a secondary coil with compensation circuit, i.e., the VA, is connected to the secondary inverter.
- In the case of three stages, after the secondary inverter comes the DC/DC converter whose tasks is battery charging.

Reducing the number of stages could increase the total efficiency of the power conversion process and reduce the size of the EV charger. However, the employed single-stage solution needs to provide all the functionalities that are offered by the classical multi-stage solution: compliance with the grid code, stable power flow to/from the EV and proper charging of the EV battery. Utilization of the matrix converter presents a common solution, whether if it is connected to a three-phase grid [74]–[78], or a single-phase grid [34], [79], that eliminates the input rectification stage from the Fig. 2.7, and directly, from the utility grid, generates the high-frequency excitation voltage for the resonant circuit. Two different three-phase topologies of the matrix converter can be encountered in the literature and that are shown in Fig. 2.8. The first one shown in Fig 2.8a, requires 4 four-quadrant switches [74], i,e, a total of 8 transistors. The more common solution consisting out of 6 four-quadrant switches, i.e. a total of 12 transistors, is shown in Fig 2.8b [75]–[78]. The number of semiconductors in the classical solution depends mainly on the topology of the PFC rectifier and varies between 10 [80] and 16 [81]. Main benefit of utilizing the matrix converter topology is the elimination of the bulky DC link capacitor that exists between the PFC rectifier and the primary inverter, which leads to a reduction in the system volume. Advantage of having a matrix topology that is connected to the three-phase grid, over the topologies that are connected to a single-phase grid, is the ability to provide a constant power flow to the EV battery. From the matrix topologies connected to a single-phase grid, it is possible to differentiate between the one that is shown in Fig 2.9a [34], that has 4 four-quadrant switches, and the one from Fig 2.9b [79], that has 2 four-quadrant switches. All of the previously listed topologies of the matrix converter in IPT applications differ in the number of switches, and consequentally, in their modulation strategies and voltage capabilities. A core comparison between them is given in Table 2.1.

Recently, topological solutions that could replace the matrix converter have been proposed. In [82], authors propose a series connection of a buck-type PFC 3-ϕ Unfolder that is followed by a T-type converter for energizing the primary side of the IPT link. This topology is depicted in Fig. 2.10a. Proposed solution is unidirectional, has high efficiency, can be made modular for reaching high power levels, and it is intended for a single-phase IPT system. The DC link that exists in this solution is considered soft as the DC link voltage is not rigid, rather it has big ripple as the capacitance values of the DC link capacitors are relatively low. For this reason, the proposed solution is considered as a single-stage solution, although it is made by a cascade connection of two converters - low frequency voltage Unfolder with the task of rectifying the grid voltages, and T-type inverter with the task of generating high-frequency voltage excitation for the IPT link and with the task of ensuring PFC and low THD of the grid currents.

Similar approach to the previous one is seen in [83], that puts forward a system based on SWISS-DAB converter that is shown in Fig. 2.10b. The main differences comparing it to the Unfolder topology are the employed modulation strategy of the T-type inverter, and the bidirectionality feature that the SWISS-DAB system possesses. This system, as well as the previous one, are intended for being connected to a three-phase grid. Authors in [84] present single-stage solution for IPT EV charger, designed for a single-phase grid, based on a floating capacitor topology that behaves as an energy buffer, eliminating power fluctuation at double the grid frequency. This topology is given in Fig. 2.10c. Interfacing the grid is the low-frequency rectifier, generating a high-ripple DC voltage. After it comes the main inverter. Additional inverter is added in series with the main one, having a bulky DC link capacitor, with

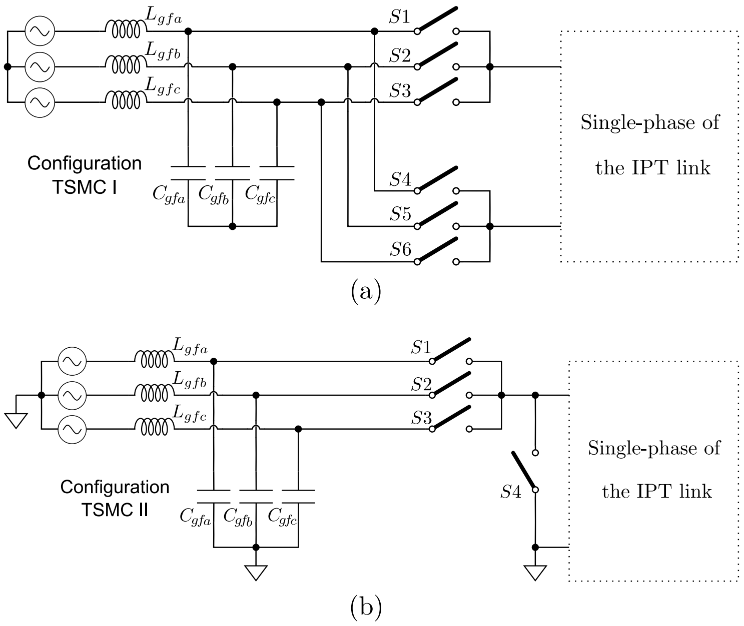

(a)

(b)

Figure 2.8: Three-Phase to Single-Phase Matrix Converter Topologies a) 6 switch b) 4 switch

the task of insuring a constant power flow to the EV battery, while the main inverter insures PFC.

Topology that is depicted in Fig 2.10d and that is discussed in [79] resembles matrix topology from Fig. 2.9b, yet it operates on different principles. In contrary to the mentioned matrix topology, where two four-quadrant switches are utilized to bring grid voltage, or zero voltage to the input of the resonant link, the proposed topology allows for higher RMS of the voltage at the resonant link as the input inductor behaves as a boost inductor, ramping-up the voltage across the capacitor connected to the high-side switch when that switch is conducting. Benefit of having higher RMS of the output voltage comes at a price of having increased voltage rating of the switches and more challenging design of the input inductor. Capacitor voltage is varying together with the grid voltage, meaning that it is not necessary to have high capacitance value for the circuit operation. Solution presented in [85] that is shown in Fig. 2.10e, is based on a bridgeless boost PFC rectifier and a full-bridge inverter, allowing for three-level voltage output. It does not comprise any four-quadrant switches. Voltage of the DC link capacitor is augmented using the energy from the boost inductor. Due to the existence of the bulky electrolytic DC link capacitor it is possible to argue whether this topology can be considered as a single-stage topology. Very similar topologies are considered in works [86], [87]. Due to lack of current-shaping control strategies of the gird current, this topology exhibits unacceptably high values of THD of the grid current.

As for the matrix converter topologies, they are widely present in the current state-of-the-art works. TSMC that is shown in Fig 2.8b is the most

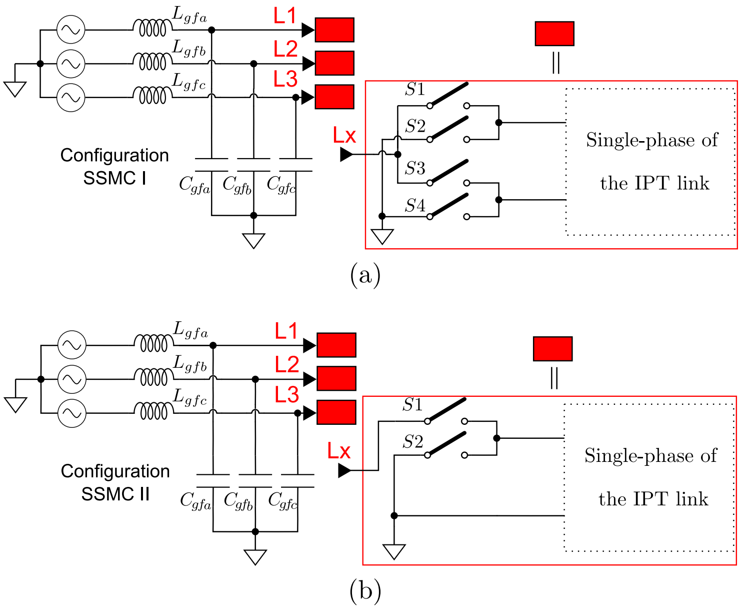

(a)

(b)

Figure 2.9: Single-Phase to Single-Phase Matrix Converter Topologies a) 4 switch b) 2 switch

Topology	Switches per phase	RMS of the output voltage (3 x 400 V, 50 Hz grid)	Constant power flow
TSMC I	6	Constant - Max. 490 V	Yes
TSMC II	4	Constant - Max. 220 V	Yes
SSMC I	4	Variable 0 V - 292 V	No
SSMC II	2	Variable 0 V - 146 V	No

Table 2.1: Comparison of the topologies from Fig. 2.8 and Fig. 2.9

commonly encountered matrix converter topology in IPT charging systems. Being that it is connected to the three-phase grid and that it allows for the highest output voltage as shown in Table 2.1, the system can be to be made for higher power levels, and it gives possibility for the constant power flow to the EV's battery. However, modulation strategy and control of such converter is a challenging task. Because it is connected to the grid, it needs to comply with the grid regulations, where critical are the ones concerning the THD of the grid currents and the resulting PF. In the current state-of-the-art, various approaches regarding the modulation of the matrix converter and control of the system can be found. In [34], the authors proposed the use of a single-phase to single-phase matrix converter with double LCC compensation strategy of the coupled coils with battery at the output of the secondary inverter. However, their control is based on controlling the high frequency current in the resonant circuit, which produces problems and limitations as the operating frequency increases. In that case, the operating frequency was 20 kHz, which is significantly lower than the current frequency range in the

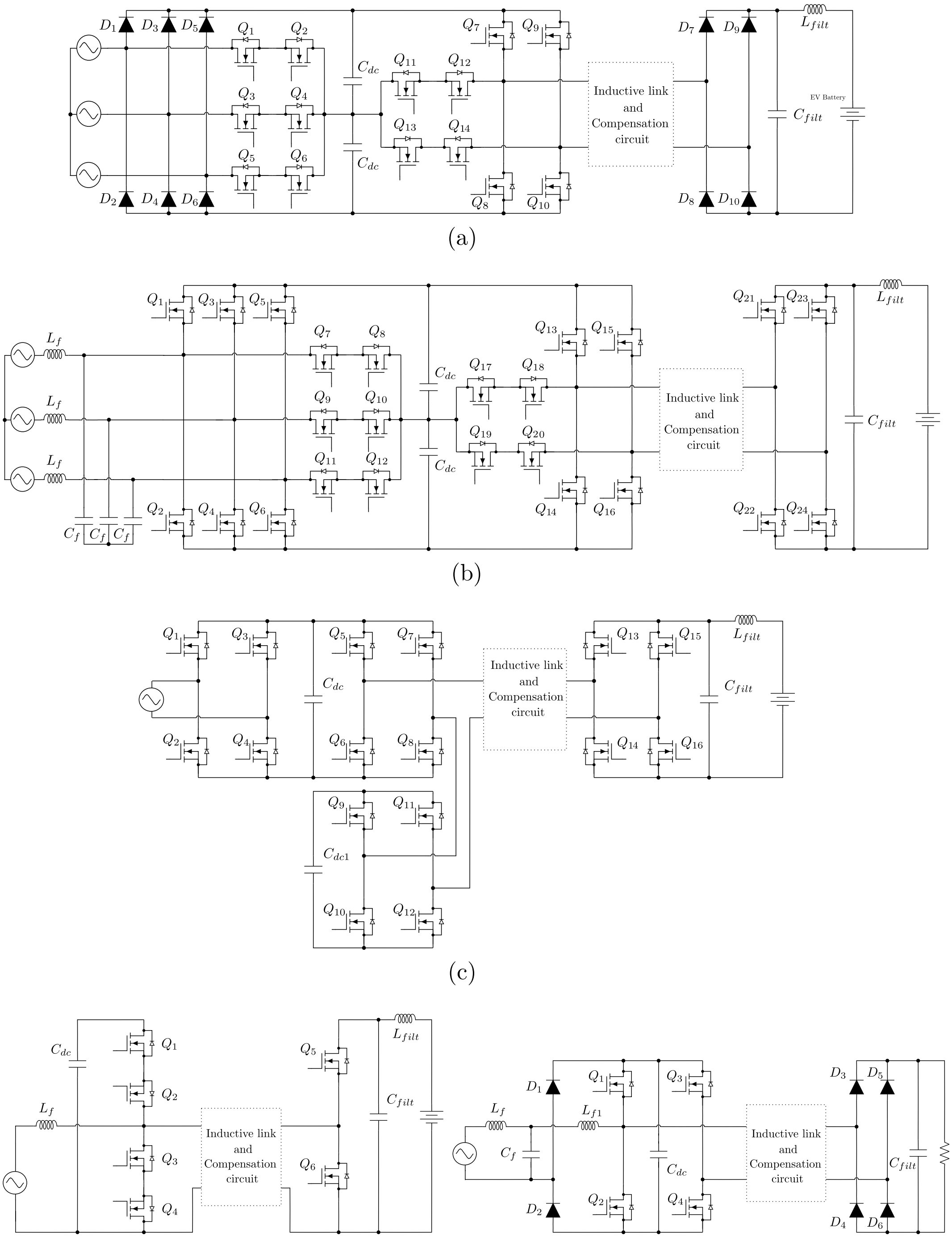

(a)

(b)

(c)

(d)

(e)

Figure 2.10: Single-stage topologies proposed in current state-of-the-art a) [82] b) [83] c) [84] d) [79] e) [85]

automotive charging applications [24]. The application of three-phase to single-phase matrix converters can be found in [74]–[78]. The IPT transfer systems in papers [76]–[78] are not bidirectional because they have a diode rectifier on the secondary. The solution in paper [74] is also unidirectional with direct placement of the resistive load at the output of the secondary and it operates with the 4 wire system, meaning the existence of a neutral wire is required. The authors of [75] suggest the use of a matrix converter with double LCC compensation strategy, and an active secondary with a battery at the output. Improved space vector modulation (SVM) with control of input power is used to control the behavior of the matrix converter, thus it requires at least two voltage and two current measurements. Due to the nature of the LCC compensation, and in order to minimize the reactive energy taken from sources, a phase shift between the matrix and the secondary inverter is fixed to $\pm\pi/2$. The synchronization problem between the primary and the secondary side [88], [89] was not mentioned in the work because the authors used a single microcontroller to control both the matrix converter and the secondary inverter, which does not correspond to inductive EV charging, where the system is controlled by two separate microcontroller units (MCUs). If this problem was considered, the system would have become significantly more complex. Approaches comprising the TSMC with the dual-active-bridge topology that are not applied in IPT systems, but are also dealing with the modulation of the TSMC can be found in [90], [91]. In these papers, the main accent is put on the modulation strategies that would decrease the losses in the TSMC and comply with aforementioned grid regulations. However, due to the difference in topologies, those modulations are not suitable for this application. A very interesting application of the IPT system comprising TSMC has been reported recently in [92] where it is used for driving permanent magnet synchronous motor. In this case, being that it is not connected to the grid, modulation of the TSMC is determined differently comparing to cases where it is connected to the grid and needs to comply with the grid code.

All of the previously discussed single-stage solutions, whether they are connected to a single-phase or a three-phase grid, have a single-phase inductive link. Oak Ridge Converter that is proposed in [93], [94], and that is portrayed at 2.11a represents a single-stage, IPT chargers, with a three-phase inductive link. The very design of a three-phase inductive link will be discussed in the following Section. Absence of four-quadrant switches makes this topology attractive, while the high resonant peak voltages on the secondary side battery filter capacitors present a significant drawback of this approach. Each of the phases of the IPT link in this case is compensated using a double-sided LCC compensation strategy. IPT system based on Integrated Three-Phase AC-DC Converter [95] is shown in Fig. 2.11b. Power transfer in this system is controlled by controlling the voltage of the DC link capacitor by using widely adopted PWM control methods of a three-phase boost rectifier. In the case of this work, system has three transmitter coils and a single receiver coil, thus it cannot be considered as a system with three-phase inductive link, as it was the case with the work [93]. IPT link is compensated using LCC-S compensation strategy.

2.3 Poly-phase IPT Chargers

When high power transfer capability is required, the usual approach is choosing a certain topology with a poly-phase inductive link. Within poly-phase IPT systems, most common are the ones with three-phases. According to their inductive link design, all poly-phase IPT systems can be divided them into:

- *Compact* poly-phase IPT systems. They are characterized by a single ferrite core bed that is common for all of the coils of the ground or vehicle assembly. Typical example of such system is present in [96].
- *Semi-compact* poly-phase IPT systems. Each of the coils has its own ferrite bed but the structure of the entire topology allows for the coils to be placed closely to one another. Examples of these coupling structures are present in [95], [97]
- *Non-compact* poly-phase IPT systems. Basically, in the terms of inductive link, they are made out of the number of single-phase IPT systems corresponding to the number of phases of the poly-phase system. Such system is present in [98].

Poly-phase IPT systems are discussed in [94], [96], [97], [99]–[106]. Authors in [96] propose several different interesting, hexagonally-shaped, coil structures for high power EV charging that are depicted in Fig. 2.12a. Each of the three phases is made similar to DD-coil, thus by rotating each of them 120^o apart, a compact structure with inter-phase decoupling is achieved. Depending on the configuration, coils are stacked into one, two or three layers. Configuration with three layers was employed in the previously commented work [94]. Similar approaches, with circular coil shapes are seen in [103], [107], that are given in Fig. 2.12b and 2.12c. Systems whose transmitter and receiver structures are based on the shapes presented in previous works, have one very useful characteristics - they are immune to the angular misalignment, i.e., system remains symmetrical in the case of angular misalignment. This is shown in [96]. This property makes such systems highly desirable for applications where only angular misalignment is expected, for example UAV charging [107]. However, if lateral misalignment is introduced to such systems, non-symmetry will arise, thus, these systems lose their advantages in applications such as EV charging. Semi-compact three-phase system, relying on three circular coils closely grouped together is presented in [101]. Single-stage solution [95], that was commented in the end of the previous Section has the same construction of the transmitter side, while on the receiver side there is a

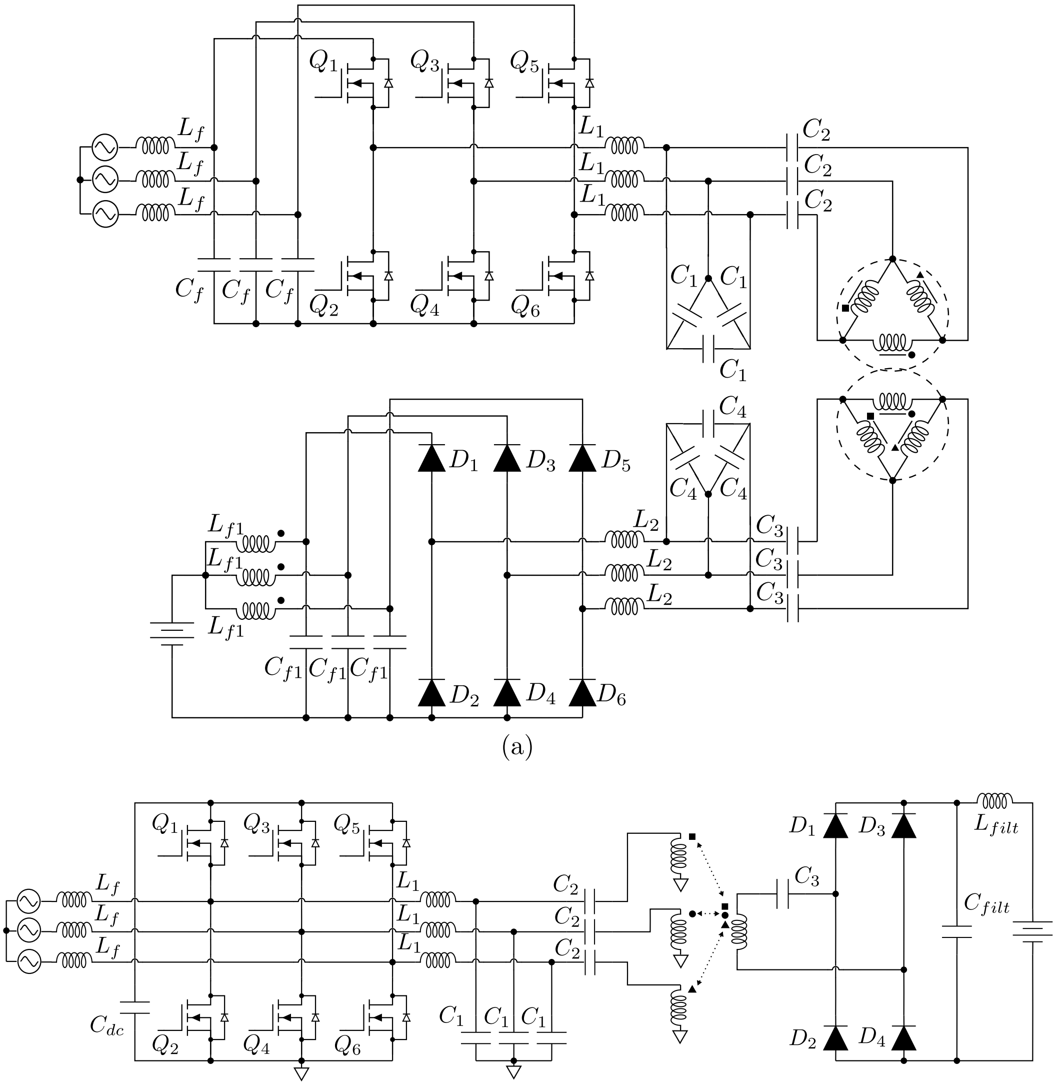

(a)

(b)

Figure 2.11: Single-stage IPT systems with three-phase inductive link a) [94] b) [95]

single coil, as it is shown in Fig. 2.12e. Articles [100], [102] present interesting compact solution for dynamic IPT charging that is shown in Fig 2.12f, with a three-phase transmitter and receiver structures. Another three-phase system, intended for wireless charging of UAVs can be seen in [106], and it is depicted in Fig. 2.12g. In [99] and [105] authors investigate different three-phase transmitter structures for omnidirectional IPT systems with a single-phase receiver, for low-power applications. These solutions are shown in Fig 2.12h and 2.12i. A three-phase IPT for high-power applications is proposed in [97] relying on adjacently placed DD coils, similar to the modular design presented in [25]. The two transmitter and receiver structure designs, proposed in this article are given in Fig. 2.12j. In the same work, authors propose a control methodology based on phase-shift for balancing the system under misalignment conditions. A high-power, semi-compact, three-phase IPT system, shown in Fig. 2.12k, is proposed in [104], giving promising results in the domain of low stray magnetic field.

The DD^{2}Q magnetic coupler structure that is out of high interest for this Thesis, was proposed in [108]. It is compact, consisted out of two, mutually orthogonal, DD coils and a Q coil, stacked one on top of another, as it is depicted in Fig 2.13a. Both transmitter and receiver structures are made in the same way. In Fig 2.13b, magnetic field generated by each of the coils of the DD^{2}Q structure is shown. As the magnetic fields are mutually perpendicular, it is possible to deduce that there is no mutual coupling between the coils of the same assembly, as well that there is no coupling between the non-corresponding coils of different assemblies, when they are in the aligned

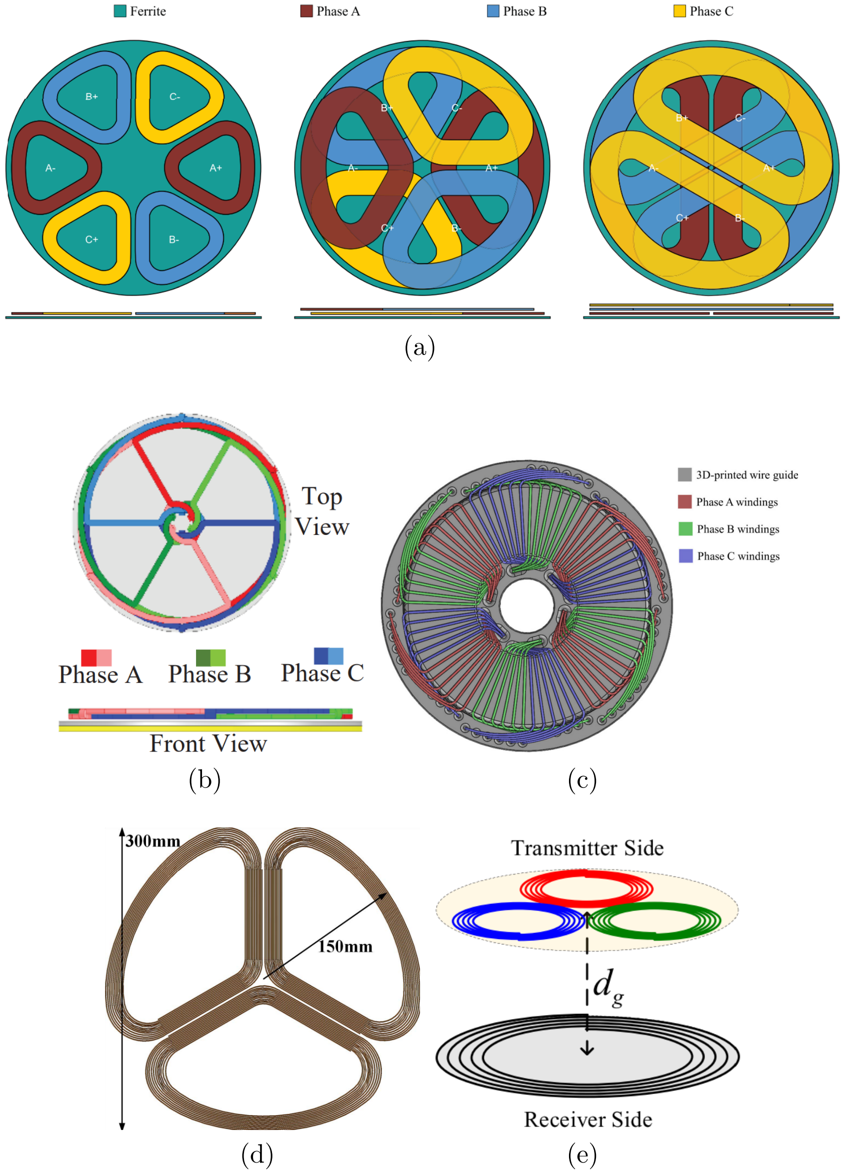

(a)

(b)

(c)

(d)

(e)

Figure 2.12

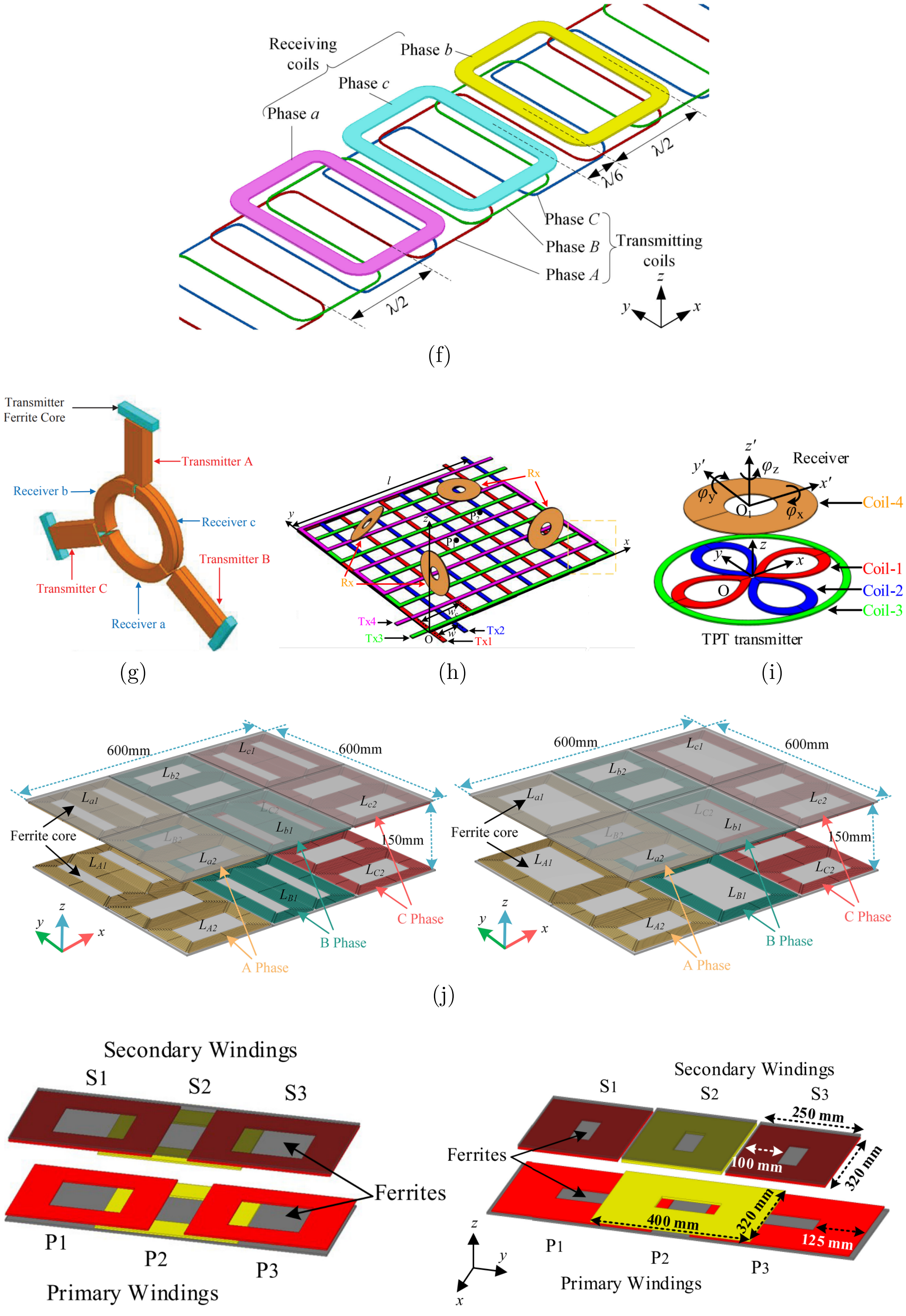

(f)

(g) (h) (i)

(j)

(k)

Figure 2.12: Three-phase inductive links proposed in the state-of-the-art a) [96] b) [103] c) [107] d) [101] e) [95] f) [100], [102] g) [106] h) [99] i) [105] j) [97] k) [104]

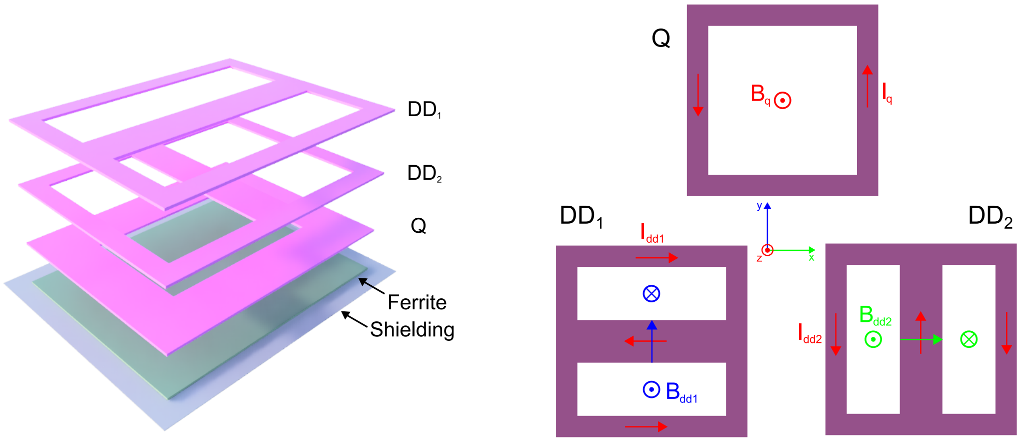

(a) (b)

Figure 2.13: DD^2Q coil topology a) Structure b) Generated magnetic fields

position. In Chapter 5 we propose a design methodology for the coupler structure based on DD^2 topology and we present a single-stage solution for wireless EV charger containing this type of magnetic coupler. More details about the properties of the DD^2 coil structure and its convenience in EV charging applications are given in the same Chapter.

Control of compact three-phase IPT systems is out of interest as well, due to non-symmetries that appear in the system, when it is not in the aligned position, which is almost certain to occur in EV charging applications. The related problems can be seen in [96]. These problems are the consequence of inter-phase coupling, and they are present in all of the compact three-phase IPT systems. Proposed solutions to balance the three-phase IPT system when it is not aligned can be seen in [97] and [98], [109]. While in [97] and [109] authors propose phase-shift adjustment of the primary voltages, in [98] an approach based on variable duty cycle of the primary voltages is present.

2.4 Synchronization between the transmitter and receiver

When speaking about the bidirectional IPT chargers for EV applications, the question of synchronizing the converters that energize transmitter and receiver sides is out of high importance. Since the entire system is made out of two physically separated parts, existence of two microcontrollers is mandatory, as it is given in Fig 2.14. One of them is placed on the ground, controlling the converter that powers the ground assembly, while the second one is on board the vehicle, managing the operation of the corresponding converter.

In order for the system to function properly, it has to operate at a certain,

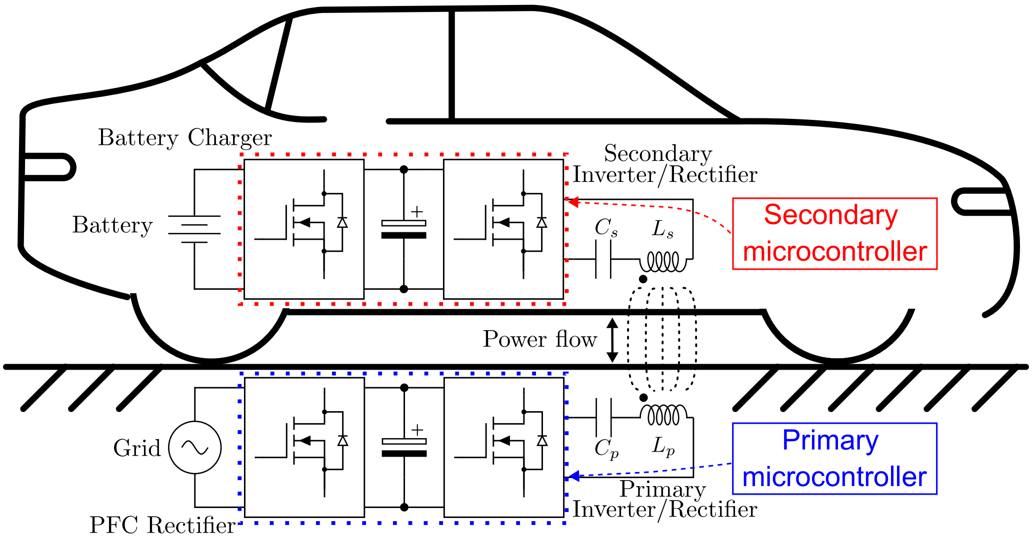

Figure 2.14: Placement of the microcontrollers that control the converters

predefined frequency. If there is only one active converter in the system, it is the one dictating the operating frequency since it is the only source of excitation. Adding a second source of excitation to the system may be problematic from the point of view of the system functionality if its operating frequency is different to the one of the first source. The case of majority of bidirectional IPT EV chargers is a typical example for this phenomenon.

Operating frequency of a converter that is controlled by any contemporary microcontroller is defined within a certain routine that is being executed withing the code that is constantly running on the given microcontroller. It is expressed in multiples of a unity clock cycles of the considered microcontroller. A unity clock cycle of a microcontroller is determined by the oscillating frequency of a component called crystal oscillator that is part of the microcontroller board. The error in the expected frequency of the crystal oscillator depends on:

1. Production tolerance - Variation during the manufacturing process
2. Temperature tolerance - Changes in frequency due to the temperature variations
3. Aging - Frequency drift over time.

The microcontroller manufacturer provides the maximum error tolerance expressed in parts per million (ppm). For the contemporary microcontroller boards this value is usually less or equal to ±50 ppm. Having in mind the clock frequencies that are in range between 10 MHz to 200 MHz, although the relative tolerance is small, this means that the absolute difference in microcontroller operating frequencies goes up to several Hertz. This difference in

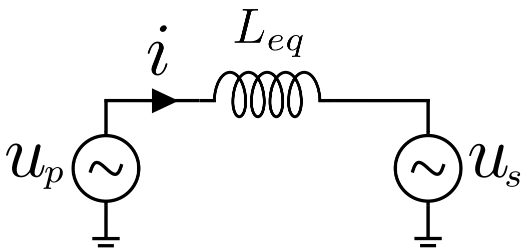

Figure 2.15: Equivalent circuit used for analyzing the phenomenon of different converter operating frequencies

clock operating frequencies of microcontrollers that control the system causes the difference in converter operating frequencies, thus it leads to the undesired system behavior, resulting into the system malfunction if it is not compensated for.

In order to get a better comprehension of the given phenomenon, it is going to be investigated in more detail. First, it is necessary to determine the electrical circuit that will be analyzed and that, from the general perspective, accurately describes the IPT applications. Without loss of generality, let us analyze the schematic given in Fig. 2.15. Namely, this is a dominantly used circuit to describe the bidirectional IPT systems in this Thesis. For IPT systems experiencing different behavior than this one, such as gyrator behavior, analogous conclusions can be deducted from their corresponding equivalent circuits.

Primary and secondary voltage are given with the following equations:

$$u_p = V\sin(\omega_p t) \tag{2.18}$$

$$u_s = V\sin(\omega_s t) \tag{2.19}$$

Now, current i of the circuit is calculated:

$$i = \int \frac{u_p - u_s}{L_{eq}}\,dt = \frac{V}{L_{eq}}(\frac{1}{\omega_s}\cos(\omega_s t) - \frac{1}{\omega_p}\cos(\omega_p t)) \tag{2.20}$$

resulting in a waveform shown in Fig. 2.16. Power that is being transferred from the primary to the secondary side is defined by the following relation:

$$p_p(t) = u_p i = \frac{V}{L_{eq}}(\frac{1}{\omega_s}\cos(\omega_s t) - \frac{1}{\omega_p}\cos(\omega_p t))\sin(\omega_p t) \tag{2.21}$$

Finding the average value of this power on the time interval determined by the difference in the two frequencies yields the average zero value:

$$P_p = \frac{|\omega_p - \omega_s|}{2\pi}\int_0^{|\omega_p - \omega_s|/2\pi} p_p(t)\,dt = 0 \tag{2.22}$$

This means, that if no measures are taken to correct the system behavior caused by difference in the converter operating frequencies, power transfer

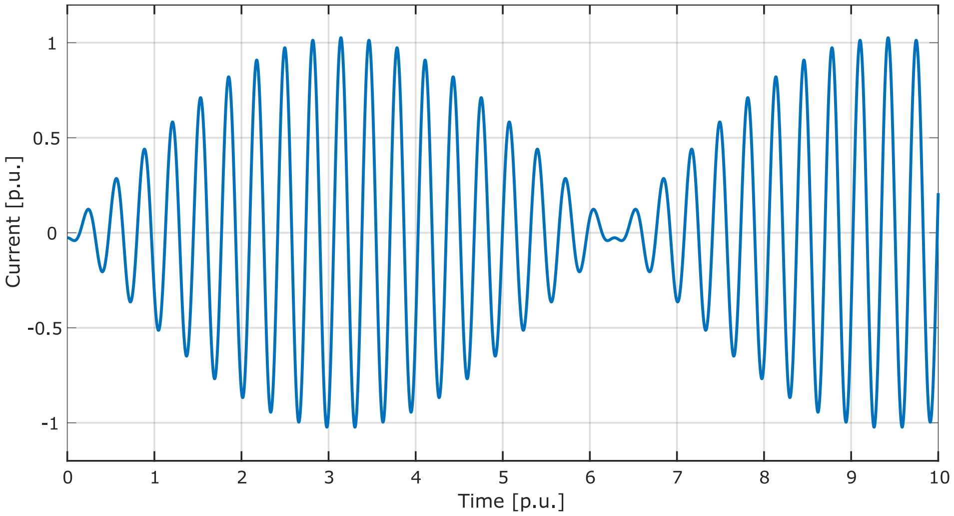

Figure 2.16: Waveform of the current from Fig. 2.15

will be impossible and system will not achieve its purpose.

Although majority of the research articles neglect this fact, there is a number of them that recognize it and propose certain solutions [88], [89], [110]–[117]. Due to high and variable transmission delays and limited data transmission rate in commercial wireless communication protocols such as Bluetooth and Zigbee, and high operating frequency of the wireless EV charging systems, these protocols are not used for solving the considered synchronization challenge [118]. They may be used within any solution for data exchange between the ground and vehicle microcontrollers, however they are not used for achieving synchronous operation.

One of the first works in this area to address the considered issue is [116], where authors rely on an auxiliary coil on the vehicle side to sense the magnetic field of the ground assembly, and perform a phased-locked loop synchronization technique. Authors of [111] analyze a complex system made out of power and driving windings with the same goal as in the previously cited work - power windings are used for transmitting power while the driving windings are used for sensing purposes. In [113] a bidirectional CPT system is analyzed. A high complexity eight-plate coupler is used, four plates are used for power transfer and the other four plates have a task of picking up relative electric fields and providing a way to synchronize converter operation. Solution presented in [116] relies on a current transformer for sensing a secondary current in a S-S compensated system and synchronizing the actions of the secondary inverter with the sensed current. Work [112] also relies on measuring the high-frequency resonant currents for achieving desired goals. Analogous method with measuring capacitor voltages is present in [110]. In [114] authors propose a methodology do enhance the synchronization strategies based on the measurement of the resonant currents and remove a potential phase error that is the consequence of the higher harmonics in this current. All of the previous works relies on measuring high-frequency current and voltages, making the electronic design complicated. Articles [75] and [89] utilize perturbation and observe method for regulating the power at the output of the secondary inverter, maintaining the approximate 90 degrees phase-shift between primary and secondary voltages in an S-S compensated system. Same method is present in [115]. This method requires estimation of the system parameters such as coupling coefficient.

What characterizes all the previously listed works is that they rely on S-S or double-sided LCC compensation strategies. This mainly influences and determines the type of synchronization that they have to apply. The main source of difference between the synchronization strategy proposed in this Thesis, in Chapter 4, and the ones from the previously mentioned articles, is the utilized compensation strategy of the IPT link, as it will be shown in Chapter 4. With this said, we can conclude with the overview of the state-of-the-art on the topics of Compensation of the IPT link, Single-stage solutions, Synchronization between transmitter and receiver and Three-phase IPT chargers. In the following Chapters, contributions of this Thesis to these fields, in the stated order, will be presented.

2.5 Conclusions

In this Chapter main challenges related to IPT EV charging are outlined:

1. **Compensation of the inductive link** - Due to low coupling coefficients between transmitter and receiver and in order to achieve high efficiency charging and desired behavior of the IPT charger, it is necessary to compensate the system.

2. **Single-stage chargers** - To be able to achieve smaller volume of the system, thus to reduce system cost and enhance reliability through lower number of components, there is a strive towards single-stage IPT chargers. However, this comes at a price of difficult controllability and lack of modulation schemes for the considered single-stage converters.

3. **Compact poly-phase IPT systems** - Increasing number of phases is a natural step towards increasing the rated power of the IPT charger. In order to make the poly-phase system compact it is necessary to consider advanced IPT coupler structures that provide decoupled operation between different phases of the system.

4. **Synchronous operation between primary and secondary converters** - In case of bidirectional EV chargers it is necessary for primary and secondary converters to operate synchronously in order for the system to function properly.

All of these topics will be discussed in the following Chapters of this Thesis where the original solutions to these challenges are proposed.

CHAPTER 3

IPT Charger with an Auxiliary Winding - Design and Tuning

> All truths are easy to understand once they are discovered; the point is to discover them
>
> Galileo Galilei

THIS Chapter proposes an IPT charger for EV applications that is compensated using an auxiliary, intermediate, winding, and three resonant capacitors. Motivated by the high efficiency of three-coil systems that are present in the state-of-the-art, and by the lack of high-power, highly efficient bidirectional solutions, in this Chapter, we propose a tuning method and a design procedure for the S-S-S compensated three-coil bidirectional IPT system intended for the EV charging applications that is given in Fig. 3.1. The considered system may contain added serial inductors on the primary and/or secondary side, as it will be explained in the following Sections. Third coil is added in order to reduce the entire system to the equivalent inductor seen between the primary and secondary sides and to provide the required reactive power for the system operation, thus lowering the current stress on the semiconductor devices and increasing the overall efficiency of the charger. Number of added compensation elements in the system is lower comparing to the most of the previously mentioned articles, thus achieving high simplicity and low volume of the system. Capacitors of the system are tuned in a manner to suit the application of high-power, bidirectional EV charger. In this Chapter we present the first original **contributions** of this Thesis:

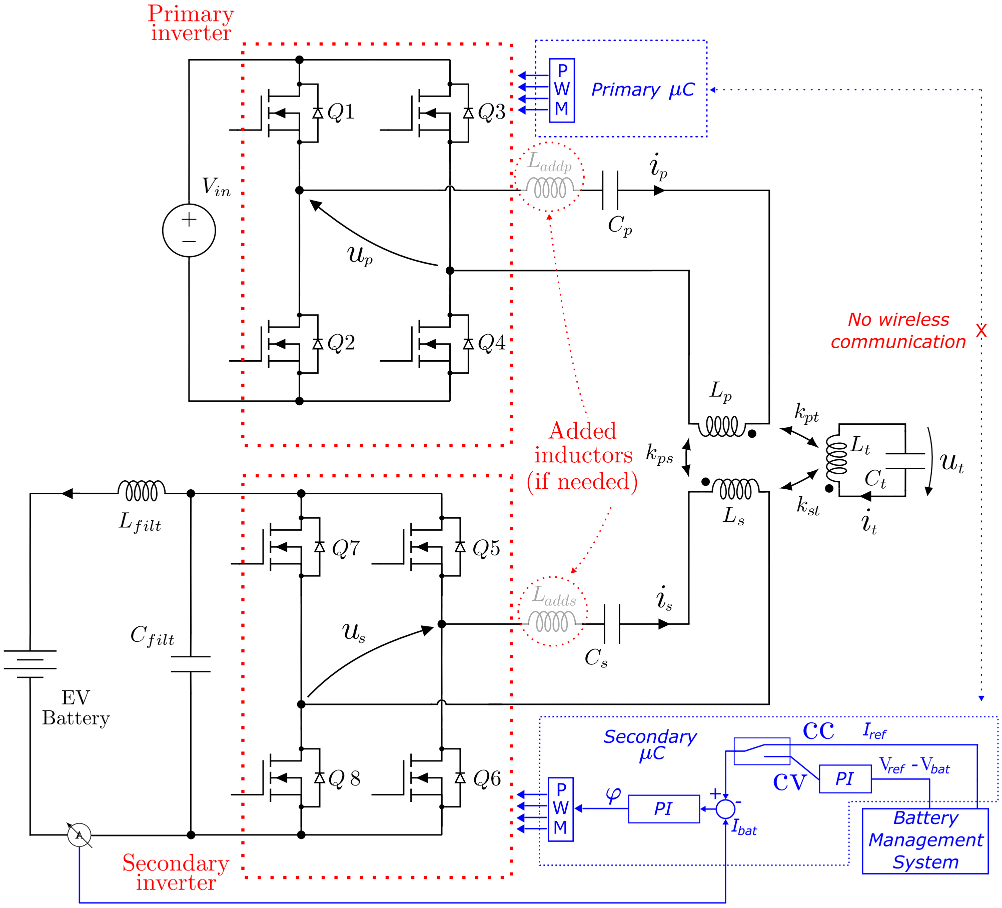

Figure 3.1: Topology of the proposed system

1. The three-coil bidirectional IPT charger for the EV applications with the S-S-S compensation technique, and tuning method for the resonant capacitors. The proposed system achieves high efficiency over a wide alignment range, allows seamless implementation of any of the previously mentioned charging methods (CC/CV, CP/CV) while being suited for the bidirectional energy transfer, allowing for seamless transitions between grid-to-vehicle (G2V) and vehicle-to-grid (V2G) modes of operation. Charging method of the charger proposed in this work is not tied with the topology itself, rather it depends on the control that is implemented on the vehicle side of the system and on the battery management system (BMS).

2. Additionally, the equivalent circuit of the three-coil system is derived and used for all the analysis that were considered, significantly improving the system comprehension comparing to the understanding provided by the mathematical model. The design procedure of the magnetic link for the proposed tuning method that emphasizes the high efficiency of the system and minimizes the weight that is being added to the vehicle.

In Section 3.1 equivalent circuit model of the three-coil system is derived. Section 3.2 explains the functionality of the proposed IPT charger. Design procedure of the system is outlined in Section 3.3. Experimental results are given in Section 3.4.

3.1 Model of the three-coil IPT system

In order to facilitate the understanding of the three-coil IPT system that is given in Fig. 3.1, an equivalent circuit will be used and parameters connecting the real parameters of the system with the parameters of the equivalent circuit will be derived. The three coupled inductors are given in Fig. 3.2a. Schematic of the equivalent circuit based on a three-winding transformer is given in Fig. 3.2b. Equations based on Kirchhoff's laws for the three coupled inductors are the following:

$$u_p = L_p\frac{\mathrm{d}i_p}{\mathrm{d}t} + L_{ps}\frac{\mathrm{d}i_s}{\mathrm{d}t} + L_{pt}\frac{\mathrm{d}i_t}{\mathrm{d}t} \tag{3.1}$$

$$u_s = L_{ps}\frac{\mathrm{d}i_p}{\mathrm{d}t} + L_s\frac{\mathrm{d}i_s}{\mathrm{d}t} + L_{st}\frac{\mathrm{d}i_t}{\mathrm{d}t} \tag{3.2}$$

$$u_t = L_{pt}\frac{\mathrm{d}i_p}{\mathrm{d}t} + L_{st}\frac{\mathrm{d}i_s}{\mathrm{d}t} + L_t\frac{\mathrm{d}i_t}{\mathrm{d}t} \tag{3.3}$$

where $L_{ps} = k_{ps}\sqrt{L_pL_s}$, $L_{pt} = k_{pt}\sqrt{L_pL_t}$ and $L_{st} = k_{st}\sqrt{L_sL_t}$. Analogous to this, equations based on Kirchhoff's laws can be written for the given equivalent circuit:

$$u_p = (L_{\gamma p} + L_\mu)\frac{\mathrm{d}i_p}{\mathrm{d}t} + L_\mu\frac{n_s}{n_p}\frac{\mathrm{d}i_s}{\mathrm{d}t} + L_\mu\frac{n_t}{n_p}\frac{\mathrm{d}i_t}{\mathrm{d}t} \tag{3.4}$$

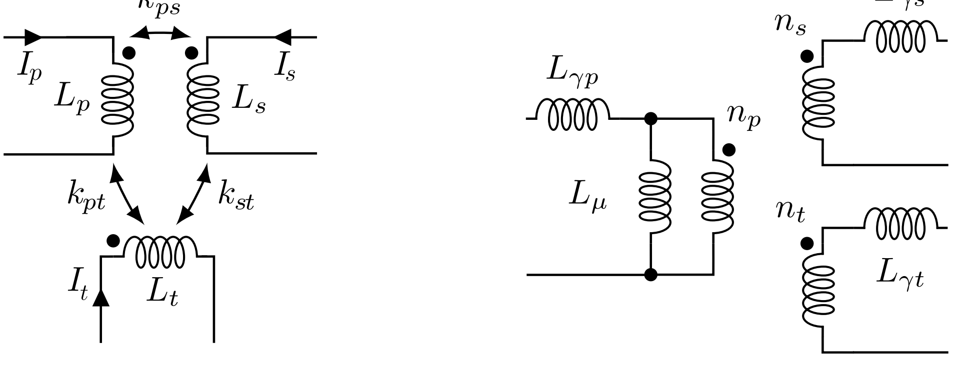

(a) (b)

Figure 3.2: a) Three coupled inductors, b) Equivalent circuit of the three coupled inductors based on a three-winding transformer

$$u_s = L_\mu \frac{n_s}{n_p}\frac{\mathrm{d}i_p}{\mathrm{d}t} + (L_\mu \frac{n_s^2}{n_p^2} + L_{\gamma s})\frac{\mathrm{d}i_s}{\mathrm{d}t} + L_\mu \frac{n_s n_t}{n_p^2}\frac{\mathrm{d}i_t}{\mathrm{d}t} \tag{3.5}$$

$$u_t = L_\mu \frac{n_t}{n_p}\frac{\mathrm{d}i_p}{\mathrm{d}t} + L_\mu \frac{n_s n_t}{n_p^2}\frac{\mathrm{d}i_s}{\mathrm{d}t} + (L_\mu \frac{n_t^2}{n_p^2} + L_{\gamma t})\frac{\mathrm{d}i_t}{\mathrm{d}t} \tag{3.6}$$

The proposed equivalent circuit does not represents a physical equivalent for the considered system, rather a mathematical one, and it should be regarded as such.

Based on the previous systems of equations (3.1)-(3.3) and (3.4)-(3.6), it is possible, by equalizing corresponding parts, to express the parameters of the equivalent circuit in dependence on the real parameters of the three coupled inductors. By doing so, one obtains:

$$\frac{n_p}{n_s} = \frac{L_{pt}}{L_{st}} \tag{3.7}$$

$$\frac{n_p}{n_t} = \frac{L_{ps}}{L_{st}} \tag{3.8}$$

$$L_\mu = \frac{L_{ps}L_{pt}}{L_{st}} \tag{3.9}$$

$$L_{\gamma p} = L_p - L_\mu \tag{3.10}$$

$$L_{\gamma s} = L_s - (\frac{L_{st}}{L_{pt}})^2 L_\mu \tag{3.11}$$

$$L_{\gamma t} = L_t - (\frac{L_{st}}{L_{ps}})^2 L_\mu \tag{3.12}$$

Fig. 3.3a depicts the previously derived equivalent circuit of the three-coil system with compensation applied, with all of the parameters taken to the primary side. The desired outcome of the compensation is given in Fig. 3.3b. The basic idea is to reduce the three-coil IPT system to the tightly coupled two-coil system, having an equivalent inductor, L_{eq}, seen between the primary and secondary sides, where power transfer is controlled like in the case of dual-active bridge (DAB) topology [119], thus achieving good controllability. This is valid for the fundamental frequency, i.e. the operating frequency of the converters. For the harmonic frequencies that are multiples of the fundamental frequency behavior of this system is different from the one of the DAB topology due to its resonant nature. The way of achieving the equality of the S-S-S compensated three-coil system and DAB at fundamental frequency is given in Fig. 3.3c. Tertiary capacitor is tuned to resonate with the self-inductance of the tertiary winding, thus compensating for the magnetizing inductance and reducing the current stress on the inverters, allowing for high efficiency of the system, while primary and secondary capacitors are tuned to partially compensate for the primary and secondary leakage inductances, thus leaving a part of them uncompensated, and the equivalent inductance is

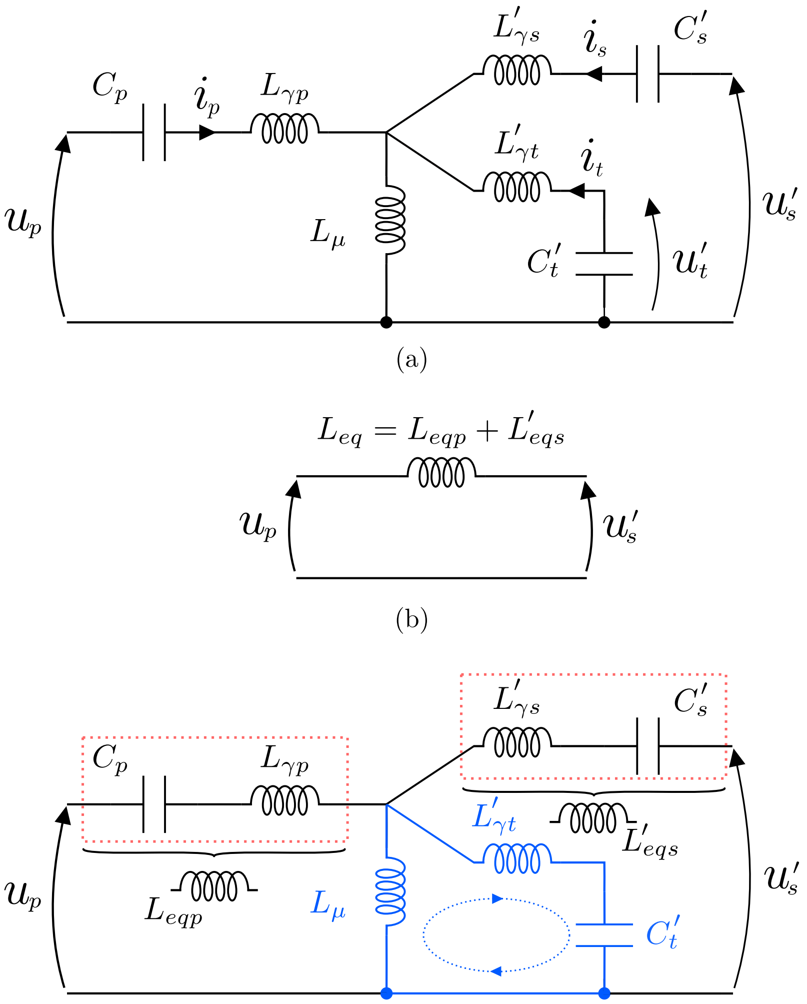

(a)

(b)

(c)

Figure 3.3: a) Compensated equivalent circuit of the three-coil inductor, b) Desired equivalent circuit, c) Operating principle of the proposed compensation strategy

seen between the primary and secondary sides. Determining the value of the equivalent inductance that is left uncompensated will be discussed in Chapter IV as this is the matter of the each IPT system in particular and depends on the voltage levels, desired power transfer capability etc. The following equations define the values of the primary, secondary and tertiary capacitors, respectively:

$$C_p = \frac{1}{(2\pi f)^2 (L_{\gamma p} - L_{eqp})} \tag{3.13}$$

$$C_s = \frac{1}{(2\pi f)^2 (L_{\gamma s} - L_{eqs})} \tag{3.14}$$

$$C_t = \frac{1}{(2\pi f)^2 L_t} \tag{3.15}$$

Basic idea of the proposed compensation strategy is stated in this Section. In Section 3.4, where the design of the system is considered, it will be shown that from the point of view of the system efficiency, it can be beneficial to take the tertiary capacitor out from the resonance. In the same Section, a guideline for determining L_{eqp} and L_{eqs} will be given. Also, external inductors can be added in series with the primary and/or secondary coils if it contributes the efficiency. However, the main principle given in this Chapter stays, the three-coil system is reduced to an equivalent inductor, that is seen between the primary and secondary side.

3.2 Topology and Functionality of The Proposed System

3.2.1 Basic Operation Principle

The system topology considered in this work is given in Fig. 3.1, while the Fig. 3.4 shows the 3-D model of the coils and their distribution in space. From the converter point of view, there are two inverters, one on the primary side and one on the secondary side. Being that the equivalent circuit of the considered three-coil IPT system is equal to the one given in Fig. 3.3b, accounting the first harmonic approximation, the active power that is going from the primary to the secondary side is equal to:

$$P = \frac{U_p U_s'}{2\pi f L_{eq}} \sin\varphi \tag{3.16}$$

where U_p and U_s' are RMS values of the 1^{st} harmonic of the primary voltage and of the secondary voltage taken to primary side, while φ is the phase-shift between the primary and secondary voltages. Controlling the power level and flow direction in this system is possible in several ways:

1. By varying the duty cycle of the inverters, values of the first harmonic of the primary and secondary inverters voltage will change, thus influencing the power level.

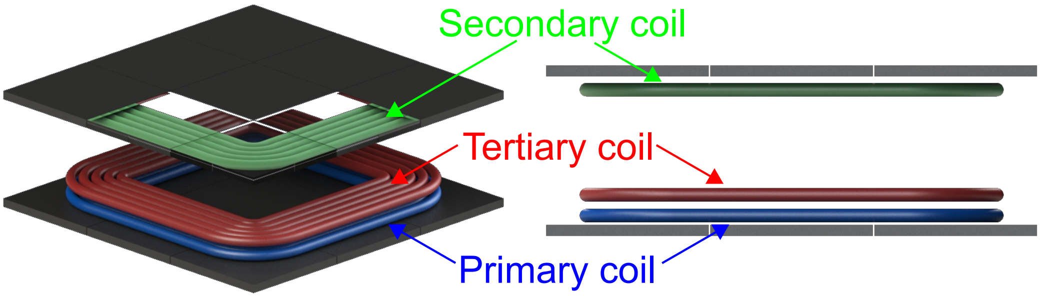

Figure 3.4: 3-D model of the proposed three-coil IPT system

2. Changing the phase shift between the primary and secondary voltages changes both power level and direction of the power flow, thus in this way change between G2V and V2G modes of operation is achieved.
3. Varying the operating frequency influences the equivalent reactance seen between the two sides, meaning that a change in frequency would cause a change in the power level. However, because of the narrow range of the operating frequencies for the considered application, the operating frequency will be fixed.

Considering that the system is intended for automotive charging applications, it is required that it remains operable and efficient under the wide range of operating conditions, out of which, the most important ones are the ones considering different clearance and misalignment conditions and different battery voltage levels. Duty cycle control will be used to compensate for the changes in the system caused by deviation of the system from the nominal condition, i.e., the conditions in which the ratio of the DC voltage levels of primary and secondary side corresponds to the transfer ratio defined in equation (3.7). Depending on the topology of the entire system, it may also be possible to vary the input voltage of the primary inverter, however in this work we will consider it invariable. Control of the phase-shift will be used for achieving the desired power flow and switching between G2V and V2G modes of operation.

As the system is composed out of two physically separated parts, two microcontroller units (MCUs) are necessary, one to control the primary inverter and other to control the secondary inverter. Problem of synchronizing the two MCUs in IPT applications can be encountered in the literature [120], [121]. This problem will be analyzed more in detail in the following Chapter, where a synchronization strategy based on the control of the secondary inverters current is proposed, that is free of any wireless communication between the primary and secondary MCUs. In this way the IPT system is seen as a controllable current source that pumps current into the battery, while the pumped current is being equal to the reference one provided by the EVs battery management system (BMS). This provides a possibility to implement any of the charging methods mentioned in the Introduction. As the BMS has the measurements of the battery voltage and current [122], to implement CV or CP charging methods only one control loop with a PI controller is to be added to the BMS, output of which is the current reference provided to the secondary MCU, given in Fig. 3.1. During the charging process, once the battery voltage reaches its defined maximum value, the CV charging period starts. During this period, the reference for the battery current is not provided directly by the BMS, rather by a PI controller with task of maintaining the battery voltage constant. Once the battery current drops below certain predefined value, it is considered that the battery is charged and the charging process is brought to a stop. Implementation of the pulsed-current and

CC charging does not require any additional control loops. In this way, the considered system mitigates the complex hybrid structures mentioned in the Introduction as the way to achieve the desired charging method, rather it is achieved by the appropriate control of the given system.

3.2.2 V2G Mode of Operation

One of the key features of the proposed EV charging concept is the bidirectionality feature that is permitted by the employed converter topology. It is out of interest to analyze the behavior of the given system in the V2G mode of operation in order to gain a deeper insight on the functionality of the system.

First thing that can be noted from the Fig. 3.4, is that the coils are asymmetrically distributed in space, i.e., primary and tertiary coil are placed next to each other, while the secondary is placed further away, on-board the vehicle. Two different aspects of the system functionality are to be discussed: power transfer and system efficiency.

From the point of view of power transfer, system will not exhibit different behavior while functioning in V2G mode of operation. This means that because of the employed compensation, from the point of view of control, system is symmetrical in G2V and V2G modes of operation. In the previous Chapter, the three coupled inductors are equalized to an three-winding transformer. At the operating frequency, tertiary capacitor resonates with the self-inductance of the tertiary winding, leading to the equivalent circuit given in Fig. 3.3c. The equivalent inductor is seen between the primary and secondary side, determining the power transfer between the two sides accordingly to the equation (3.16). For certain values of 1^{st} harmonic of the primary and secondary voltages, a certain phase-shift φ causes a consequential active power flow from grid to vehicle, with amplitude equal to P. If sign of the phase-shift is changed to $-\varphi$, according to equation (3.16), the power flow will consequentially change sign and the power P will be transferred from vehicle to grid. The asymmetric distribution of the coils does not influence the coexistence of the power flow that arises from equation (3.16), as this equation relies on the equivalent circuit of the system that is derived in Chapter II, where spatial distribution of the coils is not relevant for the derived model.

On the other hand, the influence on the system efficiency does exist. If system was made with tertiary capacitance tuned accordingly to equation (3.15), and with equal values of L_{eqp} and L'_{eqs} the system efficiency would be the same. However, for the reasons considered more thoroughly in the following Chapter, the tertiary capacitor is to be tuned differently, causing different system efficiencies in G2V and V2G modes of operation. However, this difference in efficiency does not influence or cause difference in control mechanism. This issue will be discussed in subsection D of the following Chapter.

3.2.3 Parameters of the considered system

In the following Chapter, design of the previously described system will be analyzed. In the case of this work, the EV charger has the following parameters:

- Nominal primary DC voltage and nominal EV battery voltage equal to 800 V. Battery voltage range is [610 V, 830 V].
- Nominal power of the charger is 30 kW.
- Litz wire is designed according to [123] and it is made out of 3000 strands of 70 µm diameter, yielding the current rating of 52 Arms assuming the current density of 4.5 A/mm^2, i.e., 58 A with the current density of 5 A/mm^2 that will be considered for the tertiary coil due to its size and position.
- Outer diameter of the coil is 350 mm, as it is defined in the SAE standard [24], for the Z2 class of clearance range. Air gap between the GA and the vehicle assembly (VA) is varying between 110 mm and 150 mm (Clearance between 145 mm and 185 mm as defined in the SAE standard). Considered misalignment is ± 50 mm in both x and y direction.
- Efficiency requirements are as well taken from the SAE standard [24]. System is required to have efficiency larger than 85% in the aligned position and efficiency larger than 80% in the misaligned position. Over the alignment tolerance area, the charger has to be able to transfer at least 50% of the nominal power.

3.3 Design of the considered system

The goal of this Section is to outline the design procedure of the considered three-coil IPT system. Two criteria are main for the design: high efficiency of the system and low weight added to the vehicle. As our desire is to propose a comprehensible design procedure without brute force optimization method, in order to facilitate its understanding, the process will be done in 5 consecutive steps:

A Determining number of turns of the primary, secondary and tertiary coils, N_p, N_s and N_t.

B The analysis of the system controllability and reactive power consumption by designing the L_{eq}.

C Improving the system efficiency by eliminating higher harmonics - adding the external inductor

D Further improving of the efficiency by tuning of the tertiary capacitance

E Final assessment of the power transfer capability and efficiency of the system in the specified design space

In the following procedure, there is the requirement for calculating system losses several times. Main system losses are composed out of:

1. Conduction losses in the IPT coils and resonant circuit
2. Conduction losses in the primary and secondary inverter
3. Switching losses in the primary and secondary inverter

while the losses in the ferrite beds of the IPT coils have been neglected due to the low density of the magnetic flux. Losses are calculated using the following equations:

$$P_l = P_{cl} + P_{ip} + P_{is} \tag{3.17}$$

$$P_{cl} = I_p^2 R_p + I_s^2 R_s + I_t^2 R_t \tag{3.18}$$

$$P_{ip} = 2I_p^2 R_{ip} + A_p(I_{poff})f + B_p(I_{pon})f \tag{3.19}$$

$$P_{is} = 2I_s^2 R_{is} + A_s(I_{soff})f + B_s(I_{pon})f \tag{3.20}$$

where R_p, R_s and R_t are the AC resistances at the switching frequency of the primary, secondary and tertiary part of the resonant link, respectively. R_{ip} and R_{is} are resistances of the primary and secondary inverter, A_p, B_p, A_s and B_s are the parameters that can be extracted from the datasheet of the semiconductors, dependent on the value of the turn-off and turn-on current.

3.3.1 Determining N_p, N_s and N_t

The design of the IPT coils dominantly determines the weight that is being added to the vehicle. This determines the place of the tertiary winding, fixing it to the ground assembly (GA), on top of the primary winding, as it is shown in Fig. 3.4. The winding is designed fixing the core geometry in accordance with the current standard proposal and the winding geometry is adjusted to obtain the maximum coupling factor [124]. The very topic of coil design is extensive, incorporates several different areas such as winding geometry, core geometry, Litz wire design etc. Detailed procedure for coil design is given in Chapter V of [124] . In this work, we addressed directly only the topic of the number of turns of the windings, as it is the most important for the presented work. As we tend to keep the added weight minimal, the number of turns of the secondary coil is sought to be as low as possible. Equation (3.7) can be rewritten in the following way:

$$\frac{n_p}{n_s} = \frac{k_{pt}\sqrt{l_p}N_p}{k_{st}\sqrt{l_s}N_s} \tag{3.21}$$

where l_p and l_s are per-turn inductances of the primary and secondary coils, respectively, that have values determined by the geometry of the winding. From here it proceeds, that achieving a certain transfer ratio with a minimal number of turns on the secondary, requires that the primary winding is made with as low number of turns as possible. Limiting factor to the number of primary turns is the design of the tertiary coil. The VA rating of the tertiary coil is equal to:

$$I_{t1}^2 \omega L_t = \frac{U_p^2}{k_{pt}^2 \omega L_p} \tag{3.22}$$

Problem with having a low value the of primary self-inductance L_p is that the required VA rating of the tertiary coil is consequently large. Design of such

Parameter	Value	Parameter	Value
L_p $[\mu H]$	10.56	n_p/n_s	1.15
L_s $[\mu H]$	106.05	n_p/n_t	0.77
L_t $[\mu H]$	13.86	L_μ $[\mu H]$	8.18
L_{ps} $[\mu H]$	7.07	$L_{\gamma p}$ $[\mu H]$	2.38
L_{pt} $[\mu H]$	10.64	$L_{\gamma s}$ $[\mu H]$	99.86
L_{st} $[\mu H]$	9.191	$L_{\gamma t}$ $[\mu H]$	0.06

Table 3.1: Simulated parameters of the considered three-coil system and the parameters of the equivalent circuit in the operating point for which the system is designed

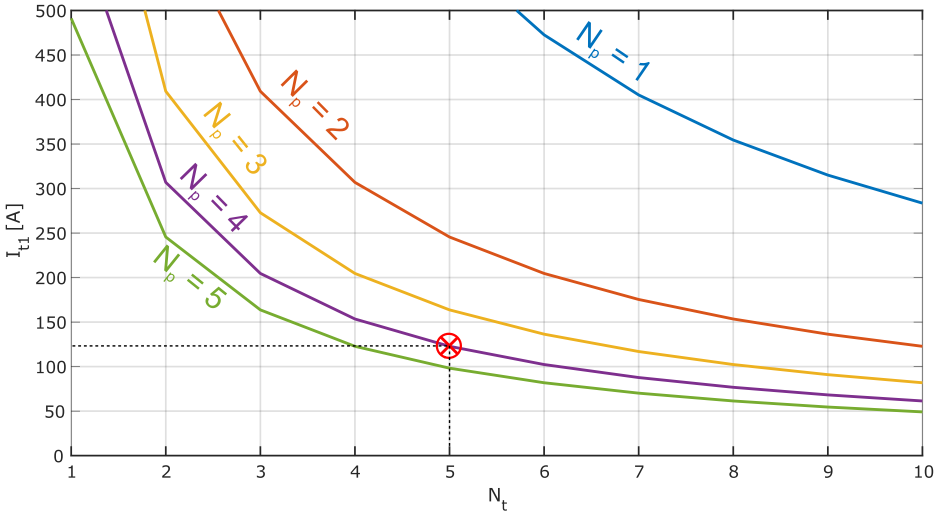

Figure 3.5: 1^{st} harmonic of the tertiary current in dependence on the number of turns of the tertiary, for different number of primary turns

a coil depends mainly on the characteristics of the available Litz wire and the physical constraints such as the coil dimensions. Fig 3.5. shows the dependence between the 1^{st} harmonic of the tertiary current on the number of turns of the tertiary, for different number of turns of the primary coil. ANSYS Maxwell was used in this process for FEA of the considered system. Based on this data and the space available for the tertiary winding, tertiary is made with 5 turns, each turn being consisted out of 3 wires in parallel. Number of turns of the primary coil is 4. These number of turns allow for minimal number of primary turns while the current in the tertiary coil has a reasonable value, enabling for a conventional design of such a coil. VA rating of the tertiary winding is 120 kVA. Current at the tertiary winding in the nominal condition is 127 A, leaving enough of the safety margin due to the potential difference between simulated values and real-life values and for the possible overcompensation of the tertiary that will be considered in subsection D of this Chapter. Number of turns of the secondary winding is determined based on the desired transfer ratio. From (3.7) it is clear that the transfer ratio will vary depending on the coupling conditions. Nominal transfer ratio is defined as the transfer ratio calculated according to (3.7), in the aligned case and air gap being equal to the mid-point from the considered range of air gaps. Nominal transfer ratio will be determined so that it is equal to the ratio between the input DC voltage and the EV battery voltage equal to the mid-point from the range:

$$(\frac{n_p}{n_s})_n = \frac{2V_{in}}{V_{batt}^{min} + V_{batt}^{max}} \tag{3.23}$$

Equalizing right-hand sides of equations (3.21) and (3.23), one obtains the number of turns of the secondary coil. Using the FEA simulation to obtain per-turn inductances of the coils and the coupling factors between them, it is determined that the required number of turns on the secondary is 13. Parameters of the simulated system and of the equivalent circuit are given in the Table 3.1. With this, the design of the coils is concluded. Coils designed in the previously described manner, allow for high efficiency of the system through ensuring a wide range of operating conditions where zero-voltage-switching (ZVS) is achievable. This topic is discussed more in-detail in subsection E of this Chapter. From the point of view of coil design, equation (3.23) determines the number of turns of the secondary is crucial as the given transfer ratio is the main parameter that influences the range of system conditions where ZVS will be possible.

3.3.2 The analysis of the system controllability and reactive power consumption by designing the L_{eq}

Once that the IPT coils are defined it is necessary to determine the primary, secondary and tertiary capacitor values. In order to do this, first, the value of the equivalent inductance L_{eq} has to be defined. Let us analyze the system using the equivalent circuit given in Fig. 3.3c. The operating condition of the considered system we will call *ideal* if the RMS values of the first harmonic of the primary voltage and of the secondary voltage taken to the primary side, U_p and U_s', are equal between themselves and in the same time equal to their maximum possible value. The system is said to operate in the *nominal* condition if the transfer ratio n_p/n_s is equal to its nominal value, while the system is transferring the nominal power P_n and working in the ideal condition. Phase-shift φ, and the equivalent inductance L_{eq} in the nominal condition are φ_n and L_{eqn}. For the system operating in the nominal condition, active power that is being transferred, reactive powers that are being given by the primary and secondary inverters and the one that is being consumed by the equivalent inductance are, respectively:

$$P_n = \frac{U_p U_s'}{2\pi f L_{eqn}} \sin\varphi_n \tag{3.24}$$

$$Q_p = \frac{U_p^2 - U_p U_s' \cos\varphi_n}{2\pi f L_{eqn}} \tag{3.25}$$

$$Q_s = \frac{U_s'^2 - U_p U_s' \cos\varphi_n}{2\pi f L_{eqn}} \tag{3.26}$$

$$Q_L = \frac{U_p^2 - 2U_p U_s' \cos\varphi_n + U_s'^2}{2\pi f L_{eqn}} \tag{3.27}$$

From equations (3.24) and (3.27), introducing that $U_p = U_s'$, one obtains:

$$Q_L = P_n \tan\frac{\varphi_n}{2} \tag{3.28}$$

For the system to operate with the minimal reactive power it is clear, from the equation (3.28). that it should be designed that in the nominal conditions $\varphi_n \to 0$. Under this condition, from equation (3.24), it follows that $L_{eqn} \to 0$ in order to have the non-zero, constant, power flow. This is the point where the first trade-off is made. On the one hand, low values of L_{eqn} will cause low requirement for reactive power and low conduction losses. However, on the other side, if L_{eqn} is too small, small changes in phase-shift will cause big changes in the power level, thus system may become hard to control and inoperable. Fig. 3.6a depicts variation of active power with the phase-shift for different values of equivalent inductance, as well as the phase shift for which the certain reference power level is achieved. In the vicinity of the nominal operating point, change of power with a change in phase-shift is given with:

$$\frac{\mathrm{d}P}{\mathrm{d}\varphi} = P_n \cot \varphi_n \tag{3.29}$$

Being that the operating frequency of the EV IPT chargers is between 80 kHz and 90 kHz, mismatch in the phase-shift caused by a potential latency of 20 ns - 50 ns is between 1° and 2°. In order to keep the potential drops or spikes in power level, caused by the small mismatch in phase-shift, between 2% and 3% of the nominal power, using equation (3.29), it is calculated that the nominal phase-shift should not be less than 30°. From Fig. 3.6b it is visible that, for

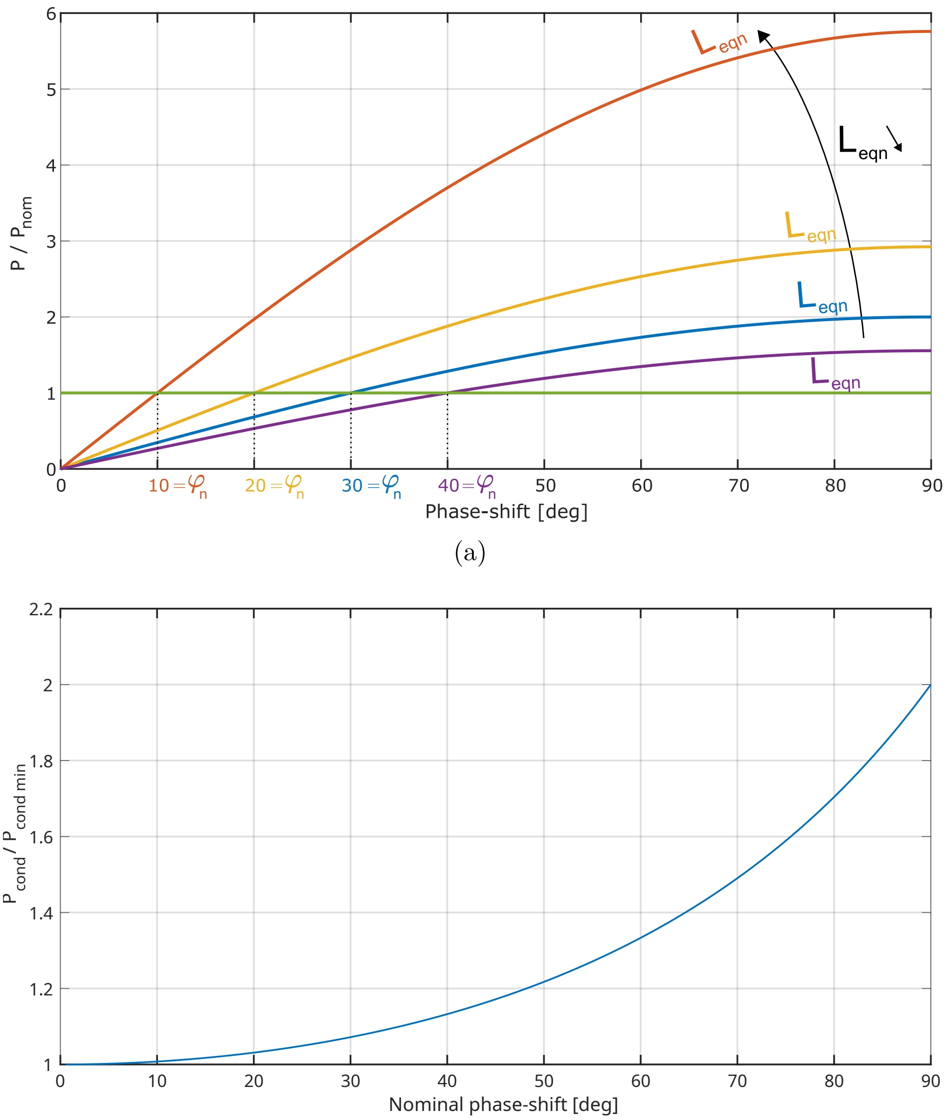

(a)

(b)

Figure 3.6

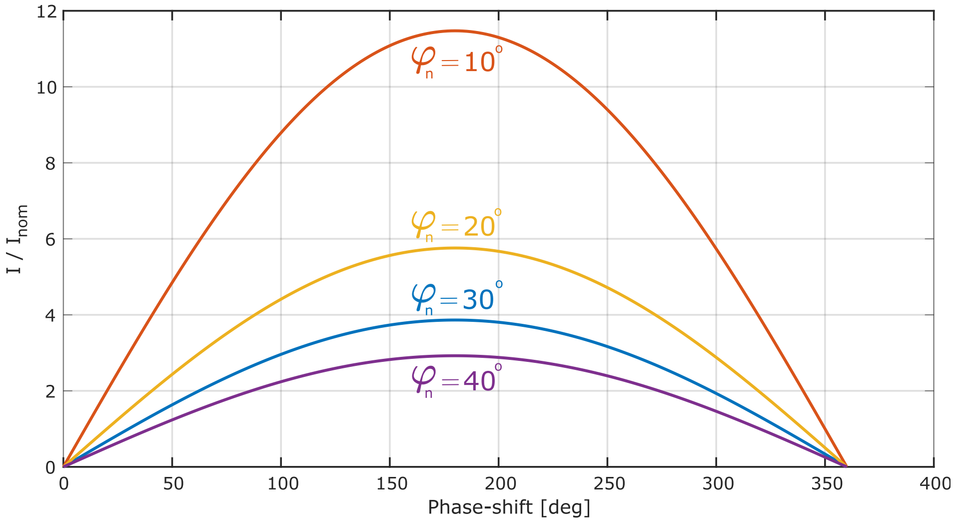

(c)

Figure 3.6: a) Change of power with change in phase-shift for different values of equivalent inductance b) Ratio between conduction losses ant the minimum conduction losses with change in phase-shift c) Ratio between current and nominal current at different phase-shifts, for different nominal phase-shift angles φ_n

this value of phase-shift, conduction losses increase caused by the reactive power are around 7%, which is acceptable. Furthermore, from the value of L_{eqn} depends the value of potential overcurrent, caused by the synchronism failure between the primary and secondary converters. The value of this current at the primary side, under nominal conditions is calculated using:

$$|I_n| = \frac{U_p}{2\pi f L_{eqn}} \sqrt{(\cos\varphi_n - 1)^2 + \sin^2\varphi_n} \tag{3.30}$$

This dependency is shown in Fig. 3.6c. If the equivalent inductance is designed in a way that the referenced power is achieved for the proposed phase-shift value of 30°, in the case of synchronism failure, maximum overcurrent is approximately equal to four times the nominal current. This is the value that contemporary SiC MOSFET transistors can endure for certain amount of time, so the protection circuit of the converters has time to react and prevent the damage. So, the value of L_{eqn} is calculated using:

$$L_{eqn} = \frac{U_p U_s'}{4\pi f P_n} \tag{3.31}$$

To have a perfect symmetry between the primary and secondary sides in nominal conditions, values L_{eqp} and L_{eqs}' from the Fig. 3.3c are chosen to be equal to half of the equivalent inductance L_{eqn}. Based on the previous discussion, the initial values of the primary, secondary and tertiary capacitors for the following iterative process are determined according to the equations (3.13) - (3.15).

3.3.3 Improving the system efficiency by eliminating higher harmonics - adding the external inductor

Due to the low values of the self-inductances of the coils, it is necessary to check for the higher-harmonic components in the primary and secondary currents. Circuit from Fig. 3.3a is linear and can easily be solved either numerically or using some circuit simulator software. For the sake of simplicity, we will omit writing the differential equations describing the system from the Fig. 3.3a. On the Fig. 3.7a the waveforms of the primary and secondary currents and voltage obtained using PLECS are shown. RMS of the primary

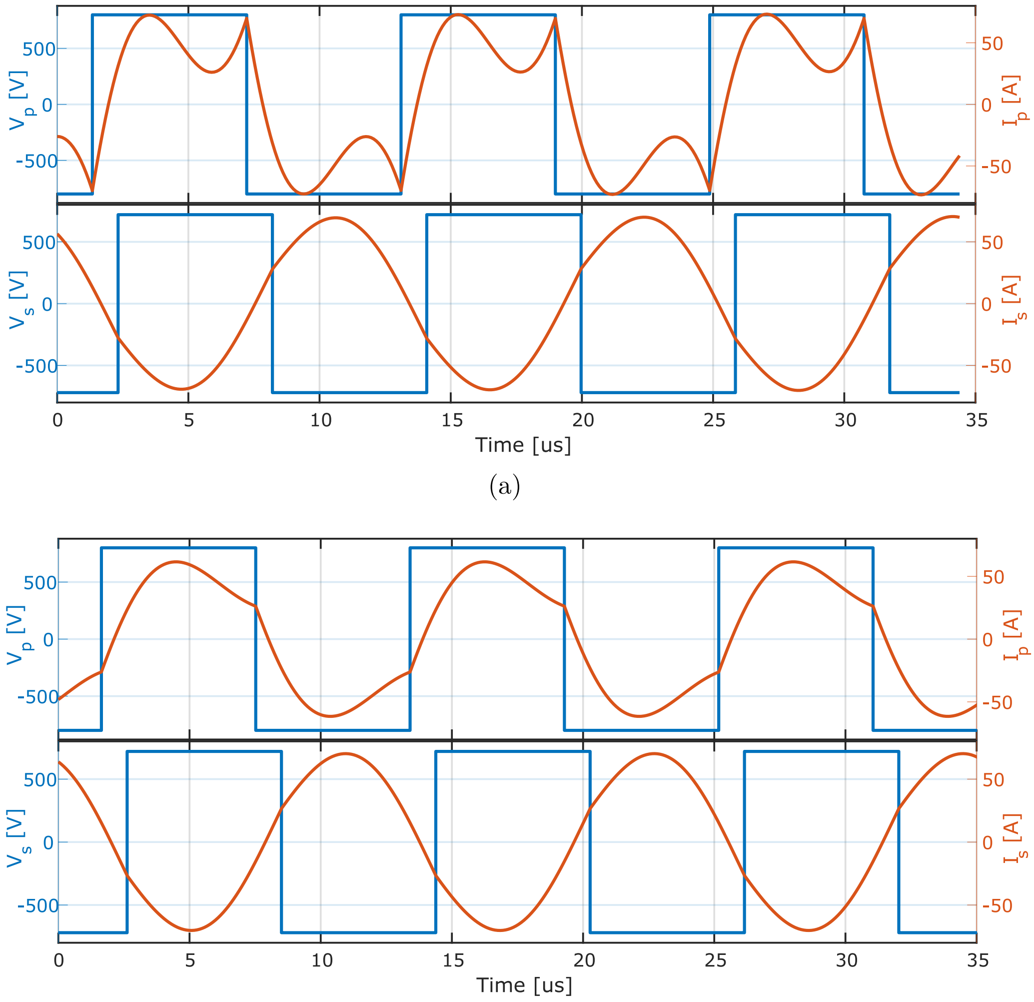

(a)

(b)

Figure 3.7: a) Primary inverter voltage and current and secondary inverter voltage and current with $L_{addp} = 5.72\,\mu\mathrm{H}$ and $C_s = 37.4\,\mathrm{nF}$ b) Primary inverter voltage and current and secondary inverter voltage and current with $L_{addp} = 30\,\mu\mathrm{H}$, $C_p = 144.5\,\mathrm{nF}$ and $C_s = 37.4\,\mathrm{nF}$

and secondary currents are 50.2 A and 51.4 A, while the instantaneous values of the primary and secondary currents in the switching transitions are, respectively, 70 A and 26.4 A. As it can be seen, the current in the switching moment in the primary inverter is substantial due to the influence of higher-harmonic components in the primary current. Adding an external inductance to the primary, while keeping the same equivalent inductance by adapting the capacitance values, is the most simple way to reduce the higher-harmonic currents in the primary. The chosen value of the added inductor depends on the permissible switching current and available space. Clearly, the higher the added inductance value is, the higher-current harmonics will be suppressed more, however the size of the added inductor represents a limiting factor. In this work we have chosen to add an inductor of 30 µH. Simulated voltages and currents in this case are given in Fig. 3.7b. Comparing this to the case shown in Fig. 3.7a, RMS of the primary and secondary currents are 44.6 A and 50.5 A, while the instantaneous values of the primary and secondary currents in the switching transitions are, respectively, 26.6 A and 26.4 A.

By now, the influence of the higher-harmonic current has been suppressed in the overall RMS of the primary and secondary currents, however it still has some influence in the switching current, i.e., the switching losses.

3.3.4 Further improving of the efficiency by tuning of the tertiary capacitance

In the previous calculus, value of the tertiary capacitance was calculated according to the equation (3.15). However, it is possible that the total system losses can be reduced more by varying the value of the tertiary capacitance. In case that the tertiary circuit is out of resonance at the fundamental frequency, i.e., it is injecting (capacitive behavior - tertiary is overcompensated) or draining (inductive behavior - tertiary is undercompensated) reactive power. The equivalent circuit or the system can be represented using an equivalent Π schematic given in Fig. 3.8. Parameters of the Π schematic are defined using the following equations:

$$L_{eq}^{\Pi} = L_{eqp} + L_{eqs}^{'} + \frac{\omega^2 L_{eqp} L_{eqs}^{'}}{Z_{eq}} \tag{3.32}$$

$$Z_{eqp}^{\Pi} = \omega L_{eqp} + Z_{eq} + \frac{L_{eqp}}{L_{eqs}^{'}} Z_{eq} \tag{3.33}$$

$$Z_{eqs}^{\Pi'} = \omega L_{eqs}^{'} + Z_{eq} + \frac{L_{eqs}^{'}}{L_{eqp}} Z_{eq} \tag{3.34}$$

First, the losses are calculated. Depending what losses are dominant, C_t is to be increased or decreased. If the conduction losses in the tertiary circuit are dominant, C_t should be decreased. If the semiconductor losses are dominant,

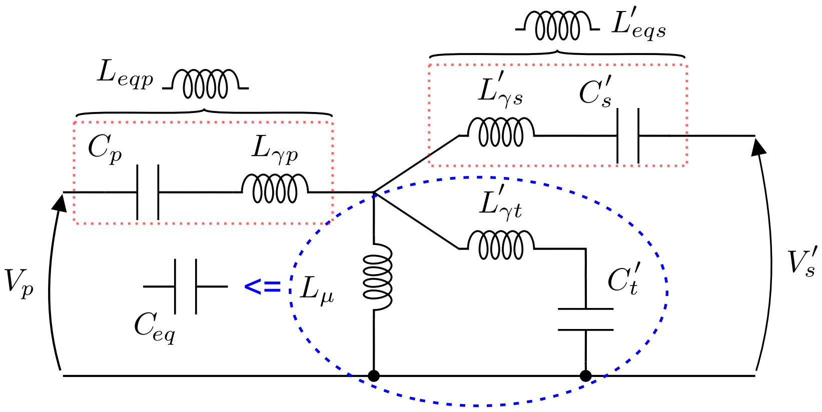

(a)

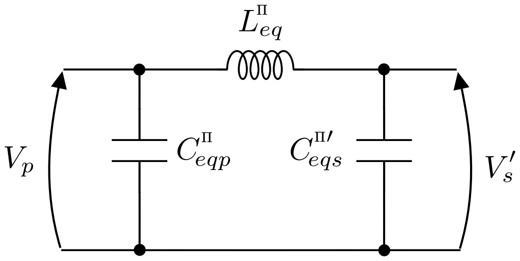

(b)

Figure 3.8: a) T equivalent circuit of the three-coil system with overcompensated tertiary winding b) Π equivalent circuit of the considered three-coil system

C_t should be increased. C_p and C_s are recalculated each time in order to keep L^{Π}_{eq} constant. The iterative process is maintained until the total losses start rising. The final values of the capacitors are C_p =144.4 nF, C_s =37.4 nF and C_t =274 nF. The proposed capacitor tuning method differs from all of the tuning methods mentioned in the Introduction as it leads to having an equivalent inductance seen between the primary and secondary sides, while most of the tuning methods from the cited works strive to achieve a resonance independent on the coupling between the coils, thus they tend towards the well-known gyrator structure via tuning the compensation capacitors to resonate with the self-inductances of the coils. The estimated efficiency of the system is more than 96% for the inverters made with G3R20MT12N transistors and for the estimated AC resistances of the primary, secondary and tertiary parts of the circuit, respectively, equal to 40 mΩ, 140 mΩ and 20 mΩ. The resistances were estimated using FEA simulations, and further improved using the experience that we have working with the mentioned type of Litz wire. The primary resistance includes for the added inductor as well. As the result of increasing the tertiary capacitance, current in the tertiary winding is increased to the 152 A and its VA rating as well to 171 kVA.

Throwing the tertiary capacitor out of resonance will reflect itself through different efficiencies of the system in G2V and V2G modes of operation.

Parameter	Value	Parameter	Value
L_p $[\mu H]$	10.62	n_p/n_s	1.96
L_s $[\mu H]$	104.4	n_p/n_t	0.77
L_t $[\mu H]$	13.92	L_μ $[\mu H]$	8.26
L_{ps} $[\mu H]$	4.22	$L_{\gamma p}$ $[\mu H]$	2.36
L_{pt} $[\mu H]$	10.69	$L_{\gamma s}$ $[\mu H]$	102.251
L_{st} $[\mu H]$	5.46	$L_{\gamma t}$ $[\mu H]$	0.06

Table 3.2: Simulated parameters of the considered three-coil system and the parameters of the equivalent circuit for the clearance of 160 mm and misalignment in both x an y axis equal to 50 mm

Namely, solving the circuit from Fig. 3.8b, the primary and secondary inverter currents will be different, causing different losses in the inverters. Also, the losses in the tertiary winding will be different due to the different voltage seen at the magnetizing inductance that is shown in Fig. 3.3c. The different voltage in two cases is caused by different inverter currents.

3.3.5 Final assessment of the power transfer capability and efficiency of the system in the specified design space

In order to verify the proposed design, it is necessary to check whether the previously designed system complies with the Design goals defined in the beginning. So, in the case of this work, the questions are:

1. Is the system capable to transfer the minimum power that is required of it in all of the possible conditions?
2. Is the efficiency of the system sufficiently high in all of the possible conditions?

To check the first question, it is necessary to simulate the system in the position with maximal clearance and misalignment. Simulated parameters are given in Table 3.2. In terms of power transfer capability, critical is the case with the minimal voltage of the EV battery. In the discussed case, the maximal power that can be transferred is equal to:

$$P_{max} = \frac{U_p U'_{smin}}{2\pi f L_{eq}} \tag{3.35}$$

Introducing the system parameters and the parameters from Table 3.2 into the previous equation, for the designed system, it is obtained that the P_{max} equals to 35.02 kW. However, due to the Litz wire current limitation of 52 A on the secondary side, power is limited to a lower value.

The matter of efficiency under various clearance values and alignment conditions is important as well. To analyze the system behavior under the misalignment and varying air gap conditions, a parameter called *relative coupling coefficient* is introduced, designated with ξ. This parameter basically represents a metric of measuring the coupling of the coils of the transmitter(primary and tertiary) with the coil of the receiver(secondary). Due to the position and sizes of the coils, it is valid to claim that the mutual inductances L_{ps} and L_{st} will change proportionally respective to their nominal values with the same scaling coefficient, with the change of the secondary coils position. The scaling coefficient, that quantifies the ratio between the L_{ps} and L_{st} in the nominal condition and their corresponding values in some other position of the secondary is the previously mentioned ξ, i.e.:

$$L_{ps} = \xi L_{psn} \tag{3.36}$$

$$L_{st} = \xi L_{stn} \tag{3.37}$$

where L_{psn} and L_{stn} are nominal values of the corresponding mutual inductances, that can be seen in Table 3.1. In the nominal position ξ equals to one. Using ANSYS Maxwell it is possible to validate that in the considered design space defined at the end of the previous Section, ξ is in range between 0.6 and 1.3. Through this, the convenience of the introduced parameter ξ is reflected, as the system will exhibit the same behavior for various air-gaps and alignment positions, as long as the considered positions have the same value of the parameter ξ. This means, that the control of the system will depend on the parameter ξ, and not on the air-gap and alignment, as the information about these two parameters is contained in the ξ. Variation of the L_{ps} and L_{st} over the alignment area, influences the transfer ratio from the equation (3.7) and the secondary leakage inductance from the equation (3.11). Thus, it changes the parameters $L_{eqs}^{'}$ and $U_{s}^{'}$ from the Fig. 3.3c. As the certain power level can be transferred for various different values of primary and secondary inverter duty cycles, each combination having a different phase-shift, finding the optimal working point of the system under non-nominal conditions is not an easy problem. However, it is always possible simplify the observed problem by fixing one of the inverter duty cycles. If ξ is lower than 1, than the duty cycle of the primary is kept constant, while the duty cycle of the secondary is reduced. In the case when the ξ is bigger than 1, it is done otherwise. In CV charging mode, as the transferred power is gradually reducing, so it is beneficial to reduce both duty cycles, as this will lead to reduction in the current of the tertiary winding. Equivalent circuit from Fig. 3.8b has been analyzed for different values of the parameter ξ. For calculating the losses, same parameters as in the previous subsection are used. Systematic circuit simulations using PLECS are conducted in order to obtain the relevant parameters of the circuit such as the RMS of the currents and the currents in switching transitions. For the values of ξ in the given range, battery voltage, power level and duty cycles of the inverters are varied to find the optimal working point for each of the possible cases of relative coupling coefficient and battery voltage levels. Expected efficiency of the system is between 90% and 97% considering all conditions. Nominal power of 30 kW is possible to achieve under higher battery voltage levels and with the higher relative coupling coefficient. For this reason, CC/CV charging method would be the most appropriate for the proposed charger topology, as it naturally requires lower power with lower battery voltages.

Hidden under the previously described method of finding the optimal operating conditions of the system for each value of ξ from the considered range, is the discussion about switching of the semiconductors. Namely, ZVS is a very important feature of the system, from the point of view of having high-efficiency and low electromagnetic interference (EMI). The inductive nature of the impedance seen between the primary and secondary contributes positively to the ZVS, as well as do the higher harmonic components in the inverter currents. As the loss of ZVS leads to significant increase in switching losses, the previously described method is naturally going to select cases with ZVS as optimal for the system operation whenever it is possible to achieve ZVS. The possibility of achieving ZVS depends on three factors: the relative coupling coefficient ξ, battery voltage and power that is being transferred. Fig. 3.9 shows the dependency of switching conditions on the ξ and battery voltage for the given power level of 30 kW.

The expected efficiency of the system is higher than it is required by the SAE standard [24], thus it can be proceeded with the prototype building and testing procedures. The entire design process described in this Section can be represented using a flowchart given in Fig. 3.10.

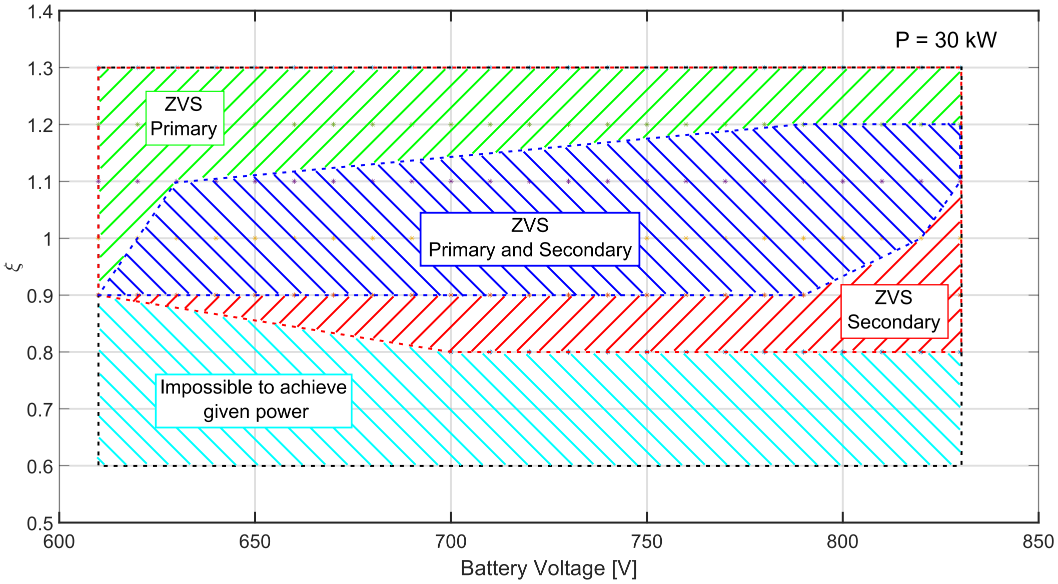

Figure 3.9: Area depicting possibility of achieving ZVS for 30 kW of power being transferred

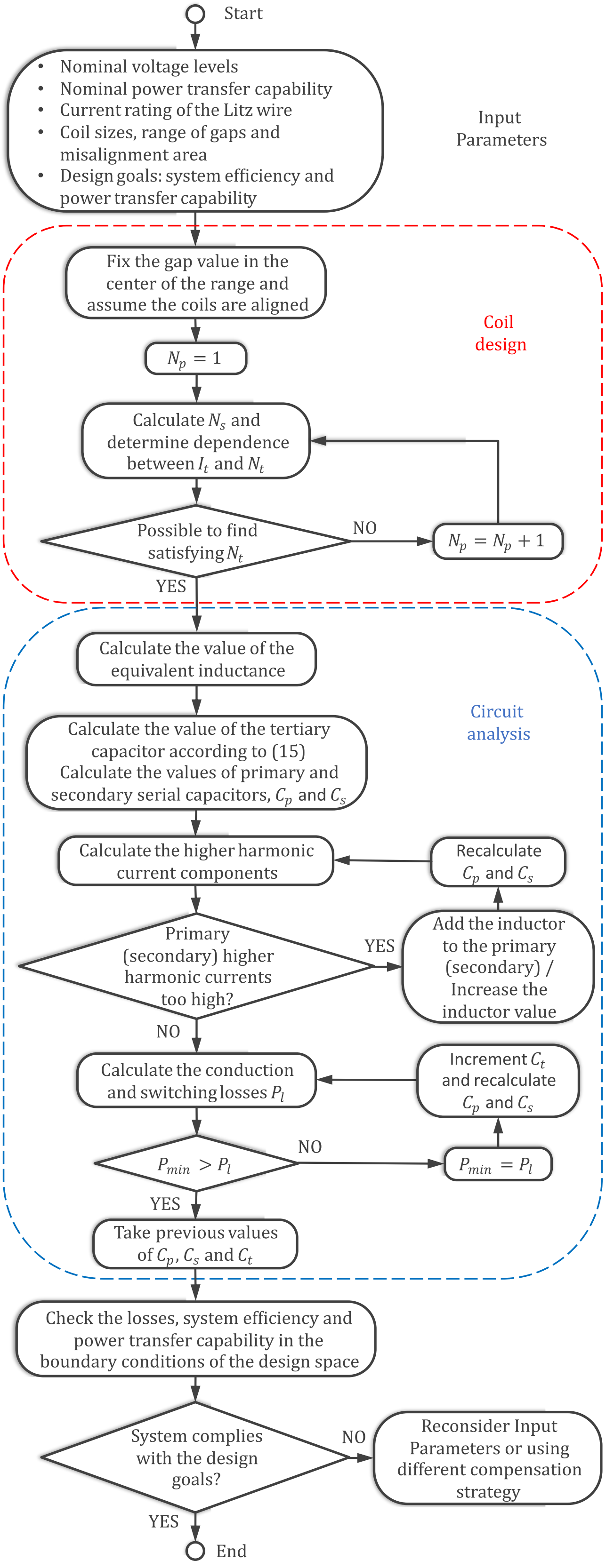

Figure 3.10: Design flowchart

3.4 Experimental results

Experimental setup built to verify the ideas proposed in this work is given in Fig. 3.11. Detailed look of the primary, secondary and tertiary coils is given in Fig 3.12. The number of turns of each winding is 4, 13 and 5, respectively. The tertiary winding shown in Fig 3.12c is made with three wires in parallel. In order to prevent circulating currents in the tertiary winding and the consequential reduction in the system efficiency, the conductors are interleaved in the way that in each turn, each of the three conductors, takes each of the three positions for one third of the turn length. In this way, the symmetricity of the conductors composing the tertiary winding is achieved. Fig. 3.13 shows the tertiary current waveforms measured in each of the three conductors of the tertiary winding, and the one measured as the sum of the three. The test was conducted with the open secondary coil and with the primary full-bridge generating a square-wave voltage with 50% duty cycle at half of its nominal voltage. As it can be seen, the currents in the three conductors of the tertiary winding are well balanced as intended. Total RMS current in the tertiary winding is equal to 84.85 A, yielding that with the nominal primary voltage it will be twice as much, giving the maximum predicted current density of 5 A/mm^2 in the tertiary conductors and the total power of the tertiary coil of 229 kVA. The 10% higher current than simulated is the consequence of the 10% difference in the tertiary winding inductance comparing to the simulations. This is the worst case scenario as there is no power transfer so the voltage on the magnetizing inductance from Fig. 3.8a is maximal. When transferring power, this current will be lower due to the voltage drop on the equivalent primary inductance L_{eqp}.

Parameter	ξ_{sim} = 1.3	ξ_{sim} = 1	ξ_{sim} = 0.6
Air gap	110 mm	130 mm	150 mm
Clearance	145 mm	165 mm	185 mm
Misalignment (x,y)	(0 mm,0 mm)	(0 mm,0 mm)	(50 mm,50 mm)
ξ_{meas}	1.27	0.99	0.62
L_p $[\mu H]$	11.49	11.49	11.49
L_s $[\mu H]$	105.43	105.67	105.81
L_t $[\mu H]$	14.89	14.89	14.89
L_{ps} $[\mu H]$	8.98	7.2	4.38
k_{ps}	0.258	0.207	0.126
L_{pt} $[\mu H]$	10.99	10.99	10.99
k_{pt}	0.84	0.84	0.84
L_{st} $[\mu H]$	11.35	8.94	5.54
k_{st}	0.286	0.226	0.140

Table 3.3: Measured parameters of the system in the three tested conditions